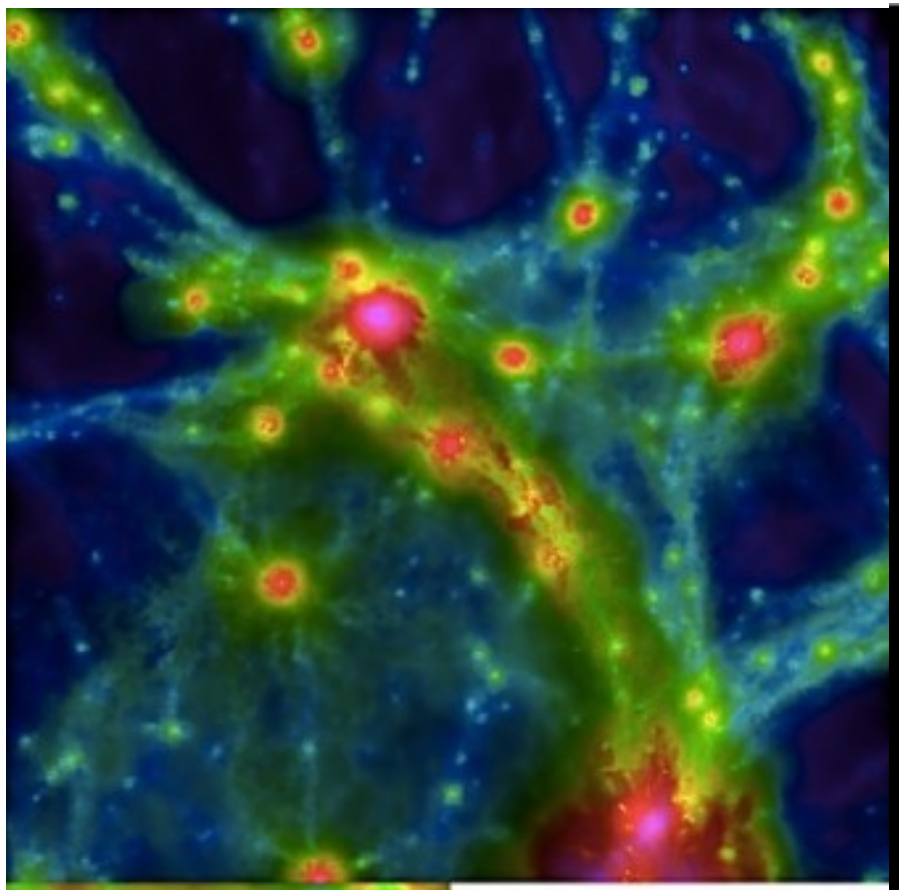

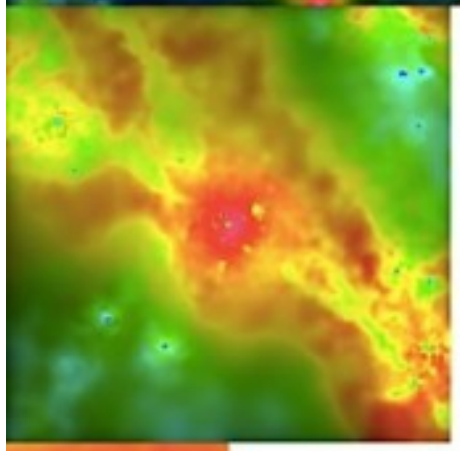

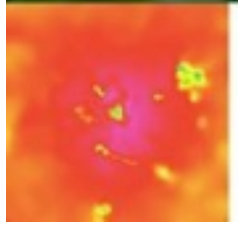

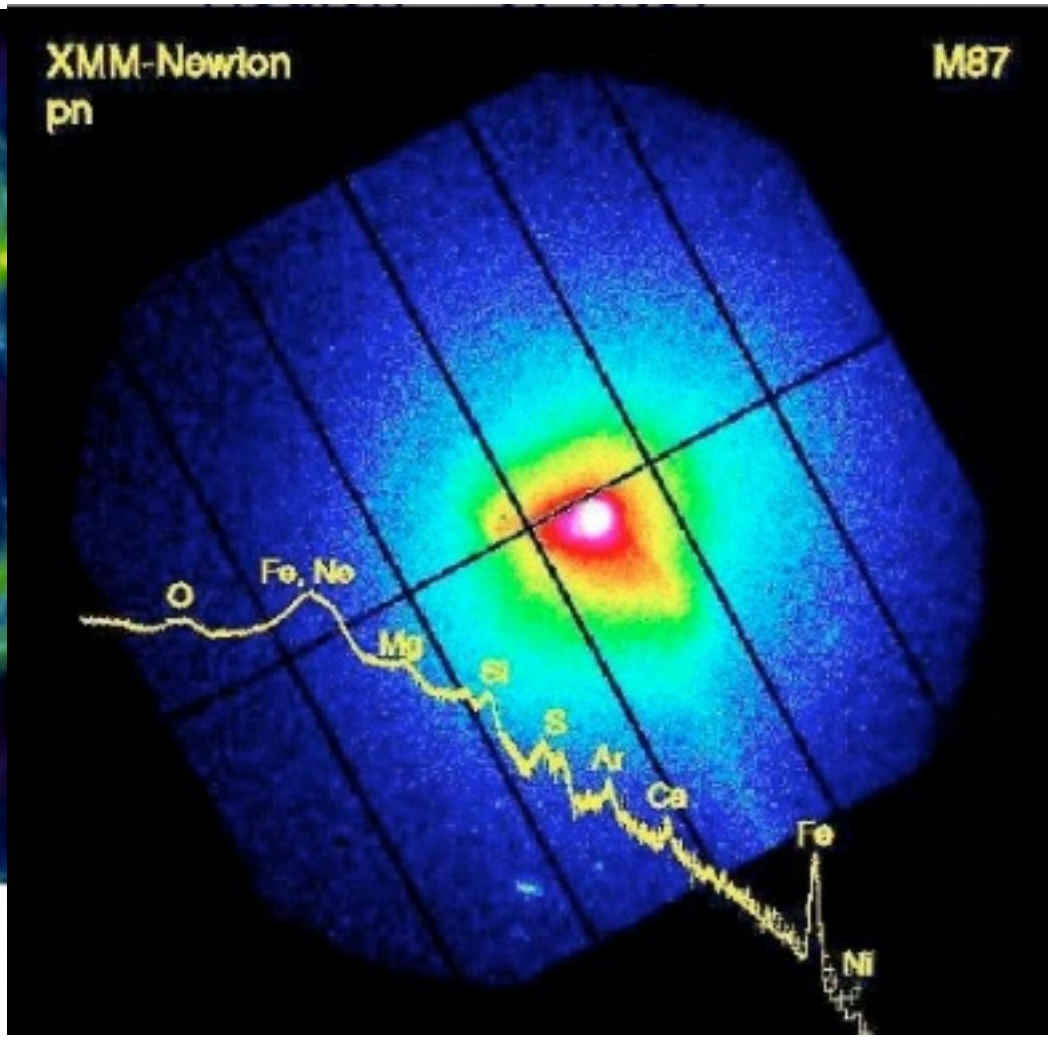

GAS HALOS: THEORY AND OBSERVATIONS

EQUATIONS GOVERNING GAS DYNAMICS

Written in physical coordinates, $\mathbf{r}$, the continuity, Euler, and energy equations are:

$$\frac{\partial \rho}{\partial t} + \nabla \cdot (\rho \mathbf{v}) = 0,$$

$$\frac{\partial \mathbf{v}}{\partial t} + (\mathbf{v} \cdot \nabla)\mathbf{v} = -\left(\nabla \Phi + \frac{\nabla P}{\rho}\right),$$

$$\frac{\partial}{\partial t}\left[\rho\left(\frac{v^2}{2} + \mathscr{E}\right)\right] + \nabla \cdot \left[\rho\left(\frac{v^2}{2} + \frac{P}{\rho} + \mathscr{E}\right)\mathbf{v}\right] - \rho \mathbf{v} \cdot \nabla \Phi = \mathscr{H} - \mathscr{C}.$$

Here ρ, $\mathbf{v}$, P, $\mathscr{E}$ are the density, velocity, pressure and specific internal energy of the fluid, respectively, and $\mathscr{H}$ and $\mathscr{C}$ are the heating and cooling rates per unit volume. For an ideal gas with an adiabatic index γ (also called the ratio of specific heats), we have $P = \rho(\gamma - 1)\mathscr{E}$.

so that $$\frac{P}{\gamma - 1}\left(\frac{\partial}{\partial t} + \mathbf{v} \cdot \nabla\right) \ln\left(\frac{P}{\rho^\gamma}\right) = \mathscr{H} - \mathscr{C}$$

In addition, the effect of gravity is given by Poisson's equation: $$\nabla^2 \Phi = 4\pi G \rho_{\text{tot}},$$

In order to study the evolution of the baryonic component using the ideal fluid approximation, one has to deal with processes that can heat or cool the baryonic gas:

Compton cooling from electron interaction with CMB photons:
When photons of low energy pass through a thermal gas of non-relativistic electrons with temperature Te , photons and electrons exchange energy due to Compton scattering. If the radiation field is a thermal background with temperature Tg ≪ Te, the net effect is for electrons to lose energy to the radiation field.

$$\frac{t_{\rm Comp}}{t} \approx 350\Omega_{\rm m,0}^{1/2} h (1+z)^{-5/2}.$$

For $\Omega_{\rm m,0} = 0.3$ and $h = 0.7$, this gives $t_{\rm Comp}/t = 1$ at $z \sim 6$. Hence, Compton cooling against the CMB is only important for gas at high redshifts.

Collisional excitation is a process in which the translational energy of a collision partner is converted into the internal energy of a reactant species.

Collisional ionization is the ionization of an ion induced by the collision of an energetic electron. On energetic grounds, it is usually the outermost electrons that are removed.

Recombination is a process by which positive ions of a plasma [capture the free [energetic] electron combine with electrons or negative ions to form new neutral atoms.

An alternative to radiative recombination is known as di-electronic recombination. In this mechanism, an electron is captured from the electron sea by an ion and the excess energy of the recombination is taken up by a second (ionic) electron which then also occupies an excited state.

Bremsstrahlung (free-free emission) is electromagnetic radiation produced by the deceleration of a charged particle when deflected by another charged particle, typically an electron by an atomic nucleus. The moving particle loses kinetic energy, which is converted into a photon.

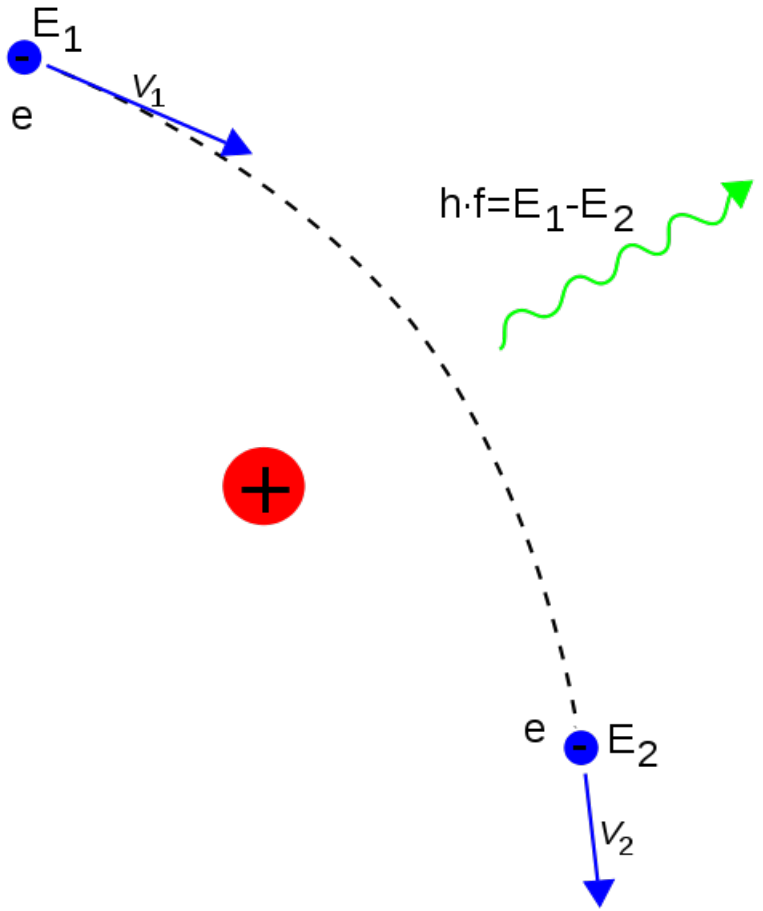

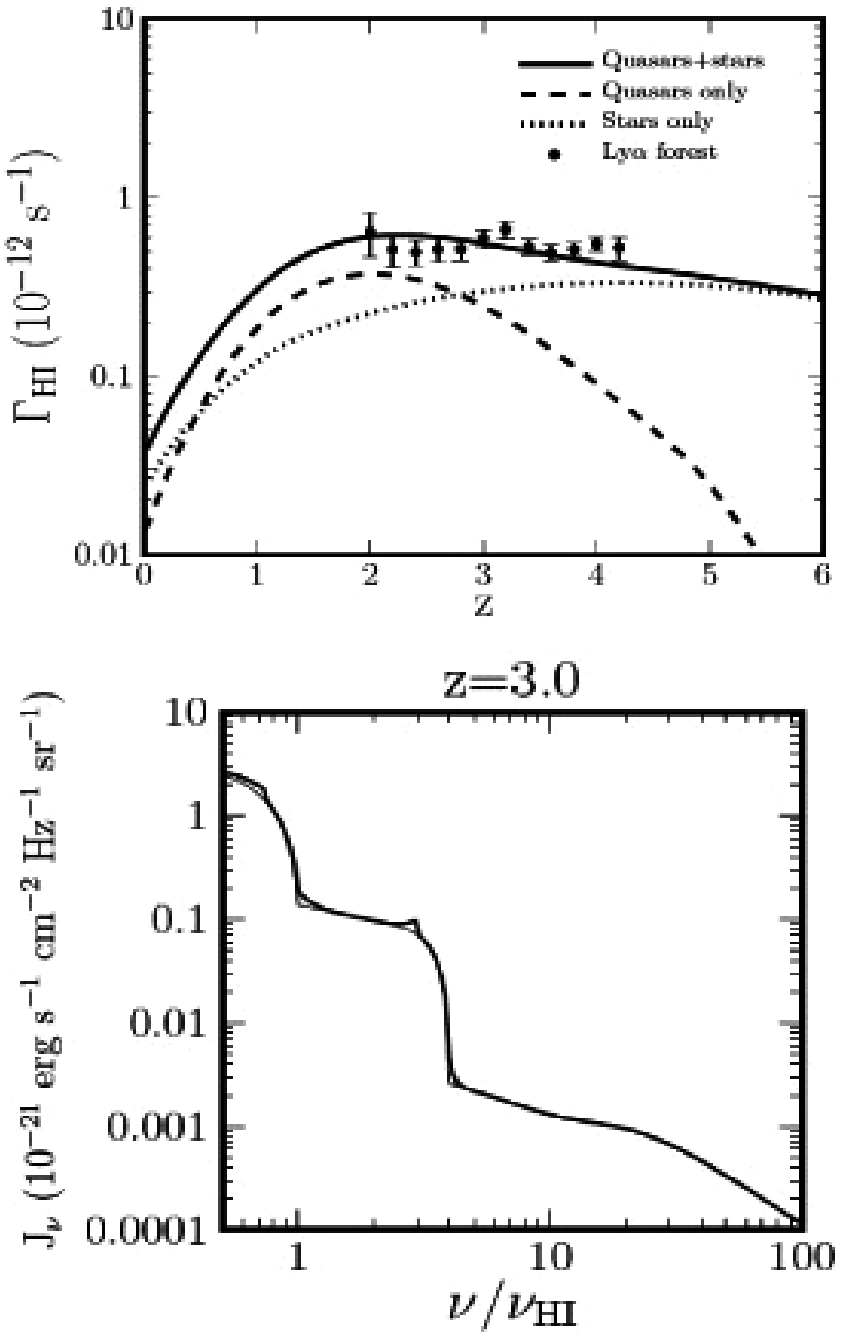

Figure 1: HI photoionization rate vs. z and detailed UV background spectrum at z=3 in our fiducial model [1].

Photo-ionization:

The interaction of electromagnetic radiation with matter resulting in the dissociation of that matter into electrically charged particles.

The combined effect of these processes is described in terms of the cooling function:

$$\Lambda(T) \equiv \frac{\mathscr{C}}{n_{\rm H}^2},$$

where $\mathscr{C}$ is the total cooling rate per unit volume and $n_{\rm H}$ is the number density of hydrogen atoms (both neutral and ionized).

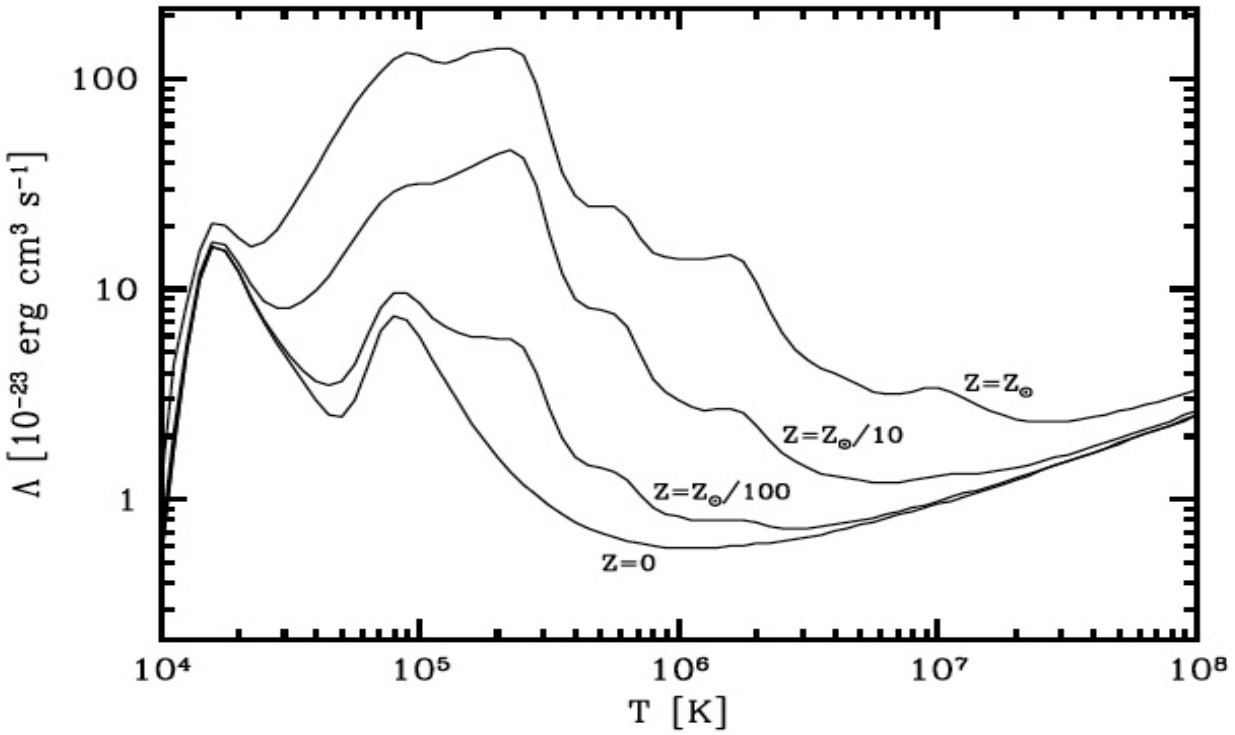

Fig. 8.1. Cooling functions for primordial ($Z = 0$) gas (assuming $n_{\rm He}/n_{\rm H} = 1/12$), and for gases with metallicities $Z/Z_\odot = 0.01$, 0.1 and 1.0, as indicated. [Based on data published in Sutherland & Dopita (1993)]

At temperatures above 10^6K, primordial gas (composed of hydrogen and helium) is almost entirely ionized, and above a few $\times 10^7$K, enriched gas (which contains also heavier elements) is fully ionized as well. The only significant radiative cooling at such high temperatures is bremsstrahlung.

For a primordial gas with $T < 10^{5.5}$K, a large fraction of the electrons are bound to their atoms, and the dominant cooling process is collisional excitation followed by radiative de-excitation; the peaks in the cooling function at 15000K and10^5K are due to collisionally excited electronic levels of H0 and He+, respectively. For an enriched gas, there is an even stronger peak at $T = 10^5$K due to the collisionally excited levels of ions of oxygen, carbon, nitrogen, etc. In an enriched gas, the cooling function is also enhanced at 10^6K by other common elements, noticeably neon, iron and silicon. At temperatures below 10^4K, most of the electrons have recombined and cooling due to collisional excitation drops precipitously. Here collisions with neutral hydrogen atoms and with the few free electrons left can excite the fine structure levels of low ions, such as OI, OII, OIII and CII.

(Note not included: If molecules (H2, CO etc) are present in the gas, collisional excitation of their rotational/vibrational levels can also contribute to gas cooling at low temperature.)

The cooling function assumes ionization equilibrium, i.e., that the densities of all ions are equal to their equilibrium values. This is only expected to be applicable if the time scales for the radiative processes in question are much shorter than the hydrodynamical time scales of the gas.

Analytic model for gas cooling in dark matter halos (White & Frenk 1991)

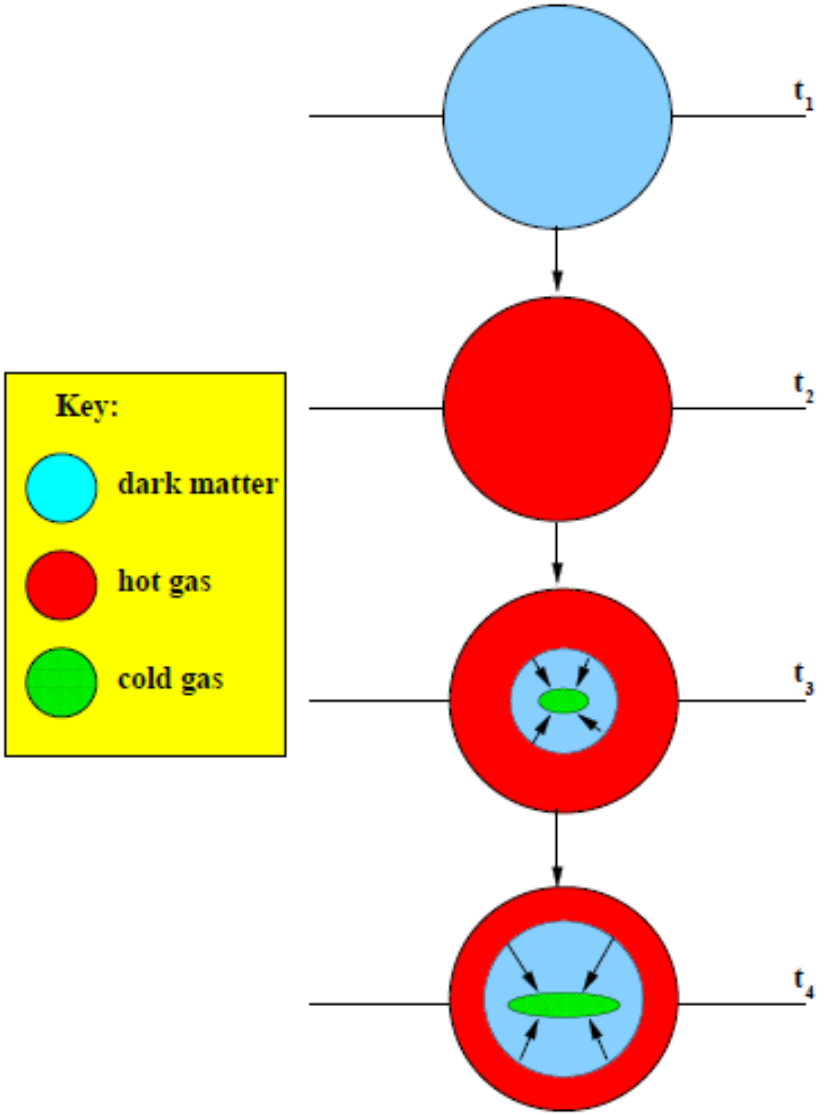

Assumption: Gas in Hydrostatic Equilibrium

$$\frac{dP}{dr} = -\frac{GM(r)}{r^2}\rho$$

ρ=density of the gas, P=pressure

– From the ideal gas law:

$$P = \left(\frac{\rho}{\mu m_H}\right)kT$$

where μ= mean molecular weight (~0.6 for an ionized plasma), m_H = mass of the hydrogen atom, k=Boltzman constant

$$\frac{dP}{dr} = \left(\frac{k}{\mu m_H}\right)\left(T\frac{d\rho}{dr} + \rho\frac{dT}{dr}\right) = -\left(\frac{GM(r)}{r^2}\right)\rho$$

$$\frac{dP}{dr} = \left(\frac{k}{\mu m_H}\right)\left(T\frac{d\rho}{dr} + \rho\frac{dT}{dr}\right) = -\left(\frac{GM(r)}{r^2}\right)\rho$$

Factor out T and ρ, multiply by r

$$\left(\frac{kT\rho}{\mu m_H}\right)\left(\frac{r}{\rho}\frac{d\rho}{dr} + \frac{r}{T}\frac{dT}{dr}\right) = -\left(\frac{GM(r)}{r^2}\right)\rho \times r$$

Then

$$\frac{kT}{\mu m_H G}\left(\frac{d\ln\rho}{d\ln r} + \frac{d\ln T}{d\ln R}\right) = -\frac{M(r)}{r}$$

Solving for M(r)

$$M(r) = -\frac{kT}{\mu m_H G}\left(\frac{d\ln\rho}{d\ln r} + \frac{d\ln T}{d\ln R}\right)r$$

If the gas is isothermal,

$$\frac{d\ln T}{d\ln r} = 0$$

Finally,

$$M(r) = -\frac{kT}{\mu m_H G}\left(\frac{d\ln\rho}{d\ln r}\right)r$$

White & Frenk assume an isothermal profile for the gas and dark matter, so that:

$$kT = \frac{1}{2}\mu m_p V_c^2 , \quad \text{or } T = 35.9\left(\frac{V_c}{\text{km s}^{-1}}\right)^2 \text{ K} , \qquad (14)$$

where μm_p is the mean molecular weight of the gas, which we fix by assuming a fully ionized gas which is 25% helium by

At each radius within the halo, the cooling time is defined as the ratio of specific energy content to cooling time:

$$t_{\text{cool}}(r) = \frac{3}{2}\frac{\rho_g(r)}{\mu m_p} kT \Big/ n_e^2(r)\Lambda(T) ,$$

Where $\rho_g(r)$ is the gas density profile and $n_e(r)$ is the electron density.

Substituting in the assumed gas profile $\rho \sim r^{-2}$ gives;

$$t_{cool}(r) = \frac{192\pi G m_p^2 r^2}{49 f_g \Omega_b \Lambda(\mu m_p V_c^2/2k)}$$

where f_g is the fraction of the initial baryon density in gaseous form.

The cooling radius is defined as the radius within the halo where the cooling time is equal to the age of the Universe. For Einstein de Sitter case, we have:

$$t_{cool}(r_{cool}) = \frac{2}{3} H_0^{-1} (1+z)^{-3/2}$$

When r_{cool} is larger than the virialized region of the halo, cooling is so rapid that **in reality**, gas will never come to hydrostatic equilibrium. The supply of gas is limited by the accretion rate onto the halo, and The time taken for accreted gas to reach the halo center, which can be roughly estimated as R_{vir}/V_C (the so-called free-fall time)

When r_{cool} lies inside the halo, infalling gas is **shock-heated** to the virial temperature, a quasi-static atmosphere of hot gas forms

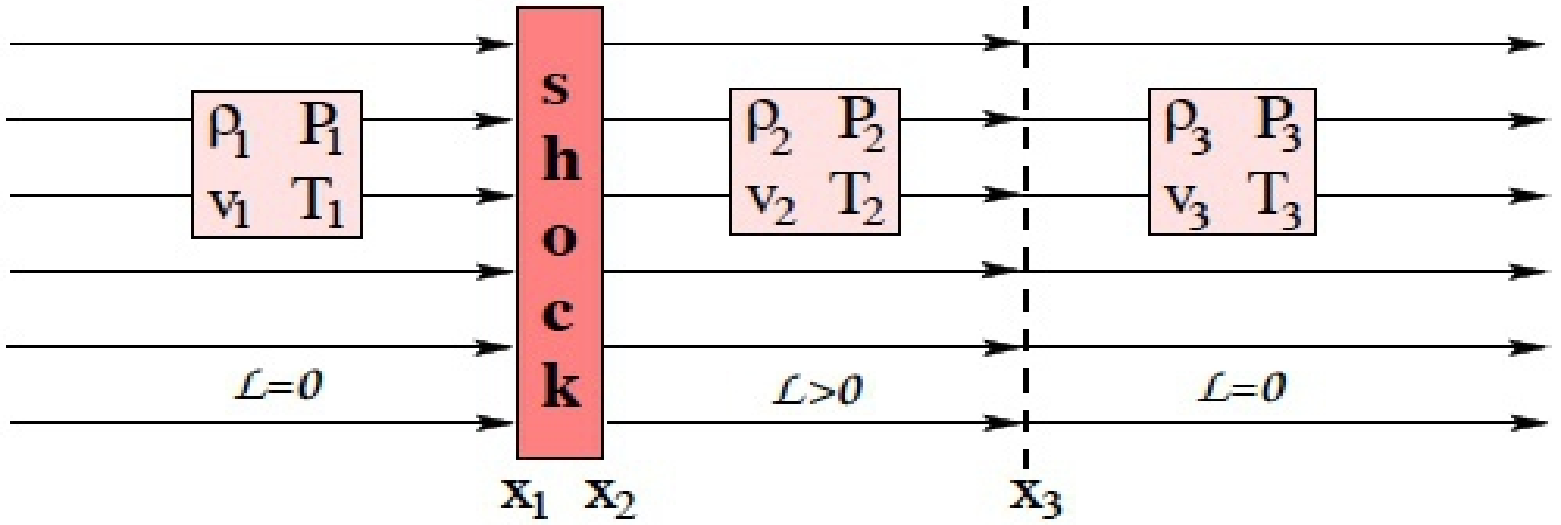

Fig. 8.3. An illustration of different regions of a planar shock. The supersonic flow in the region $x < x_1$ is shocked between x_1 and x_2 (i.e. the shock has a finite, though small, width), after which it becomes a hot subsonic flow. In between x_2 and x_3 the gas is out of thermal equilibrium resulting in net cooling ($\mathscr{L} > 0$). At $x > x_3$ the gas has cooled, reached a new thermal equilibrium, and continues to flow subsonically. The arrows indicate the direction (but not the speed) of the flow.

The compression and heating will generally push the post-shock gas out of thermal equilibrium and the gas has to cool in order to reach a new equilibrium.

Temperature

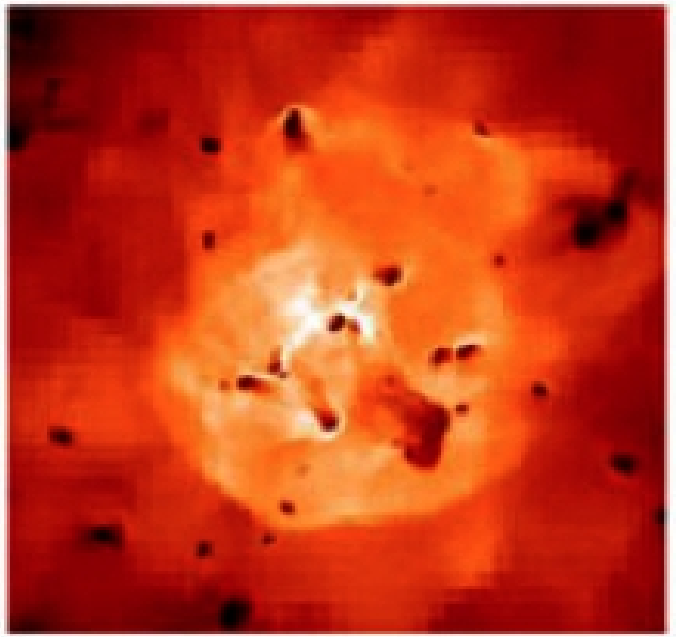

During the formation of a dark matter halo from a density perturbation, the gas initially associated with the perturbation also collapses in the gravitational potential well of the halo. However, unlike dark matter particles, shell crossing is not allowed for the gas component, and so the gas associated with a mass shell will eventually be stopped and shocked by the gaseous structure that has already collapsed. If there is no cooling, the shocked gas will remain hot, forming a hot gaseous halo in hydrostatic equilibrium in the potential well of the dark matter halo.

If the gas cools, a simple estimate of the gas inflow rate towards the center is given by:

$$\dot{M}_{\rm cool}(V_c, z) = 4\pi\rho_g(r_{\rm cool})r_{\rm cool}^2 \frac{dr_{\rm cool}}{dt}$$

$$= \frac{3}{4} f_g \Omega_b H_0 (1+z)^{3/2} \frac{V_c^2 r_{\rm cool}(V_c, z)}{G}$$

Substituting for r_{cool} , yields: $\dot{M}_{\rm cool} \propto (f_g \Omega_b)^{3/2}(1+z)^{3/4}$

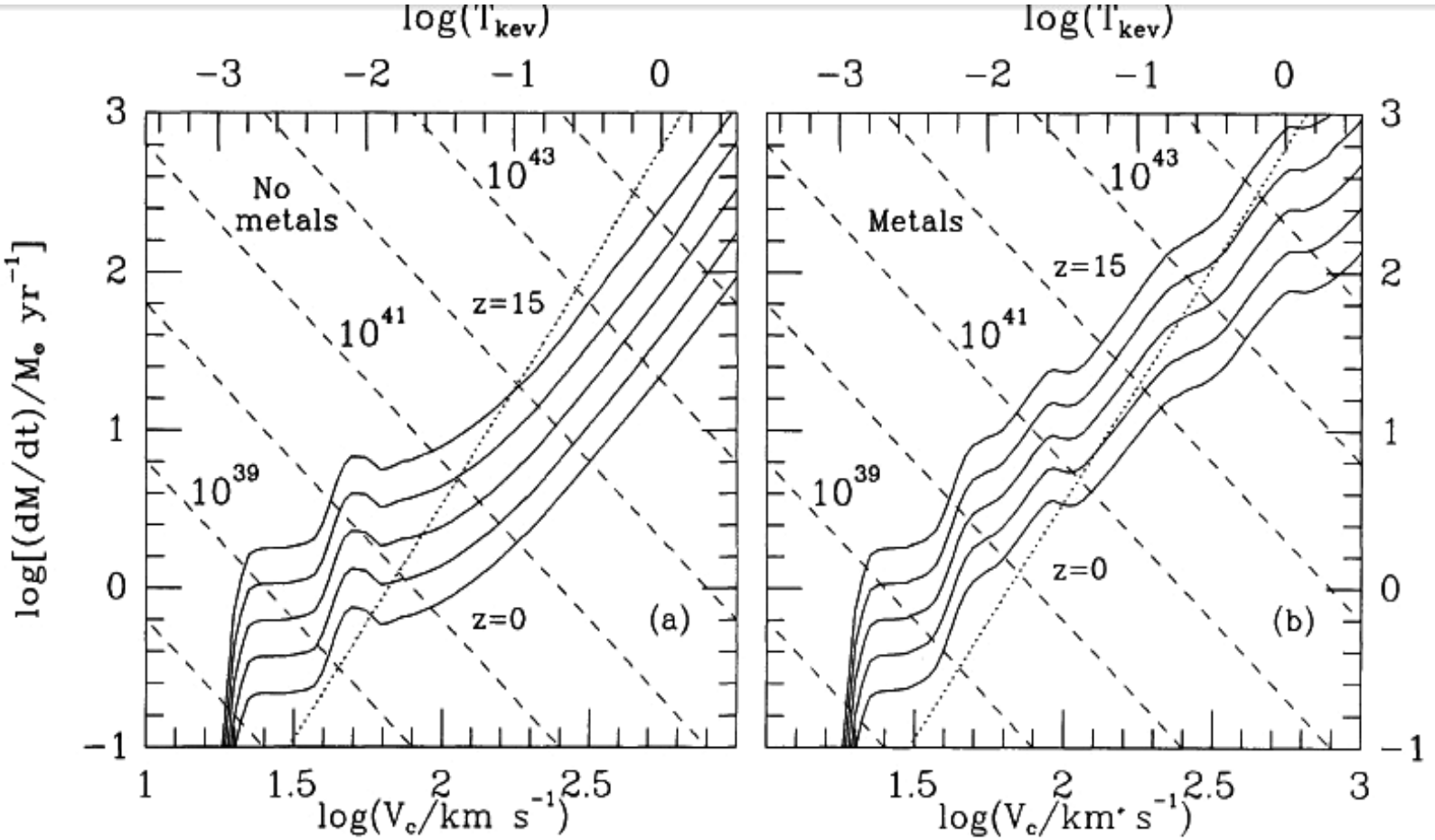

FIG. 2.—Gas infall rate and cooling rates in dark matter halos as a function of circular velocity and redshift. The infall rate (*dotted line*) is essentially independent of redshift; the cooling rates (*solid lines*) are given for redshifts $z = 0$, 1, 3, 7, and 15 (*from bottom to top*). Dashed lines give present-day X-ray luminosities in ergs s^{-1} produced by gas cooling at the given rate in each halo. The predicted temperature of this emission is given on the upper abscissa. (*a*) A cooling function for gas of zero metallicity is assumed. (*b*) A cooling function for gas enriched according to the models of § 4 is assumed. In both cases, $\Omega_b = 0.1$ and the biasing parameter b is 2.5.

Alternative approach: computational gas dynamics

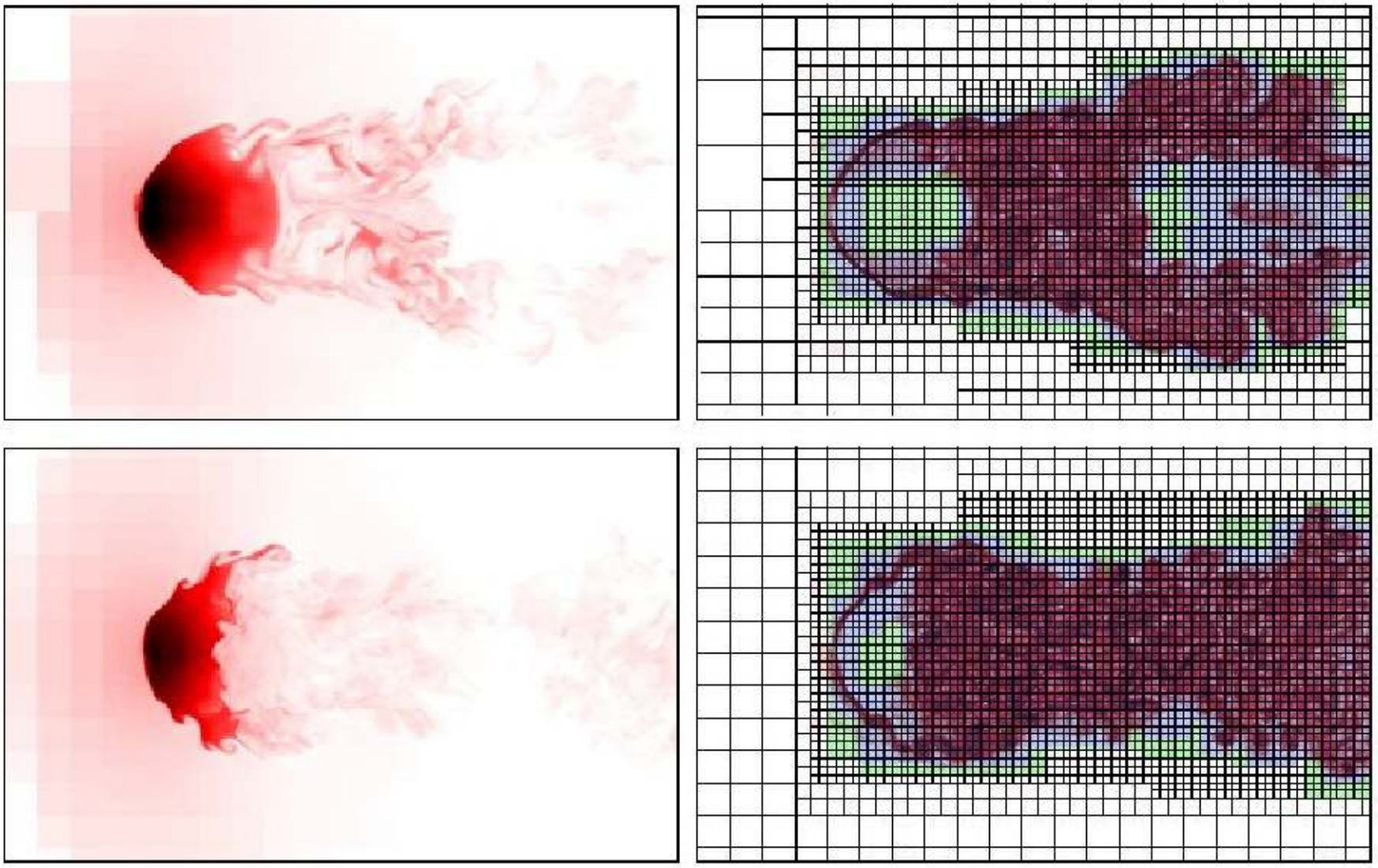

The SPH method is a particle method. Unlike the particle in cell method (PIC) (Harlow 1957, 1974, 1988), SPH does not need a grid to calculate spatial derivatives. Instead, they are found by analytical differentiation of interpolation formulae. The equations of momentum and energy become sets of ordinary differential equations which are easy to understand in mechanical and thermodynamical terms. For example, the pressure gradient becomes a force between pairs of particles.

The integral interpolant of any function $A(\mathbf{r})$ is defined by

$$A_I(\mathbf{r}) = \int A(\mathbf{r}')\, W(\mathbf{r}-\mathbf{r}', h)\mathrm{d}\mathbf{r}',$$

where the integration is over the entire space, and W is an interpolating kernel which has the two properties

$$\int W(\mathbf{r}-\mathbf{r}', h)\mathrm{d}\mathbf{r}' = 1$$

and

$$\lim_{h\to 0} W(\mathbf{r}-\mathbf{r}', h) = \delta(\mathbf{r}-\mathbf{r}'),$$

For numerical work the integral interpolant is approximated by a summation interpolant

$$A_S(\mathbf{r}) = \sum_b m_b \frac{A_b}{\rho_b} W(\mathbf{r}-\mathbf{r}_b, h),$$

where the summation index b denotes a particle label, and the summation is over all the particles. Particle b has mass m_b, position $\mathbf{r}_b$, density ρ_b, and velocity $\mathbf{v}_b$. The value of any quantity A at $\mathbf{r}_b$ is denoted by A_b.

The essential point is that we can construct a differentiable interpolant of a function from its values at the particles (interpolation points) by using a kernel which is differentiable. Derivatives of this interpolant can be obtaincd by ordinary differentiation; there is no need to use finite differences and no need for a grid. For example, if we want ∇A, we can use

$$\nabla A(\mathbf{r}) = \sum_b m_b \frac{A_b}{\rho_b} \nabla W(\mathbf{r}-\mathbf{r}_b, h),$$

One example of a commonly used interpolant is a Gaussian:

$$W(x,h) = \frac{1}{h\sqrt{\pi}} e^{-(x^2/h^2)},$$

The density is estimated everywhere by

$$\rho(\mathbf{r}) = \sum_b m_b W(\mathbf{r} - \mathbf{r}_b, h).$$

Another example is

$$\nabla \cdot \mathbf{v} = \sum_b m_b \mathbf{v}_b \cdot \nabla W(\mathbf{r} - \mathbf{r}_b, h),$$

but in this case it is better to remember the second golden rule of SPH which is to rewrite formulae with the density placed inside operators. For the previous case we write

$$\nabla \cdot \mathbf{v} = [\nabla \cdot (\rho \mathbf{v}) - \mathbf{v} \cdot \nabla \rho]/\rho,$$

so that the divergence of the velocity at particle a can be found from

$$\rho_a (\nabla \cdot \mathbf{v})_a = \sum_b (\mathbf{v}_b - \mathbf{v}_a) \cdot \nabla_a W_{ab},$$

where the notation $\nabla_a W_{ab}$ denotes the gradient of $W(\mathbf{r}_a - \mathbf{r}_b, h)$ taken with respect to the coordinates of particle a. If the kernel is a Gaussian, the contribution from particle b to the divergence of the velocity at particle a is given by

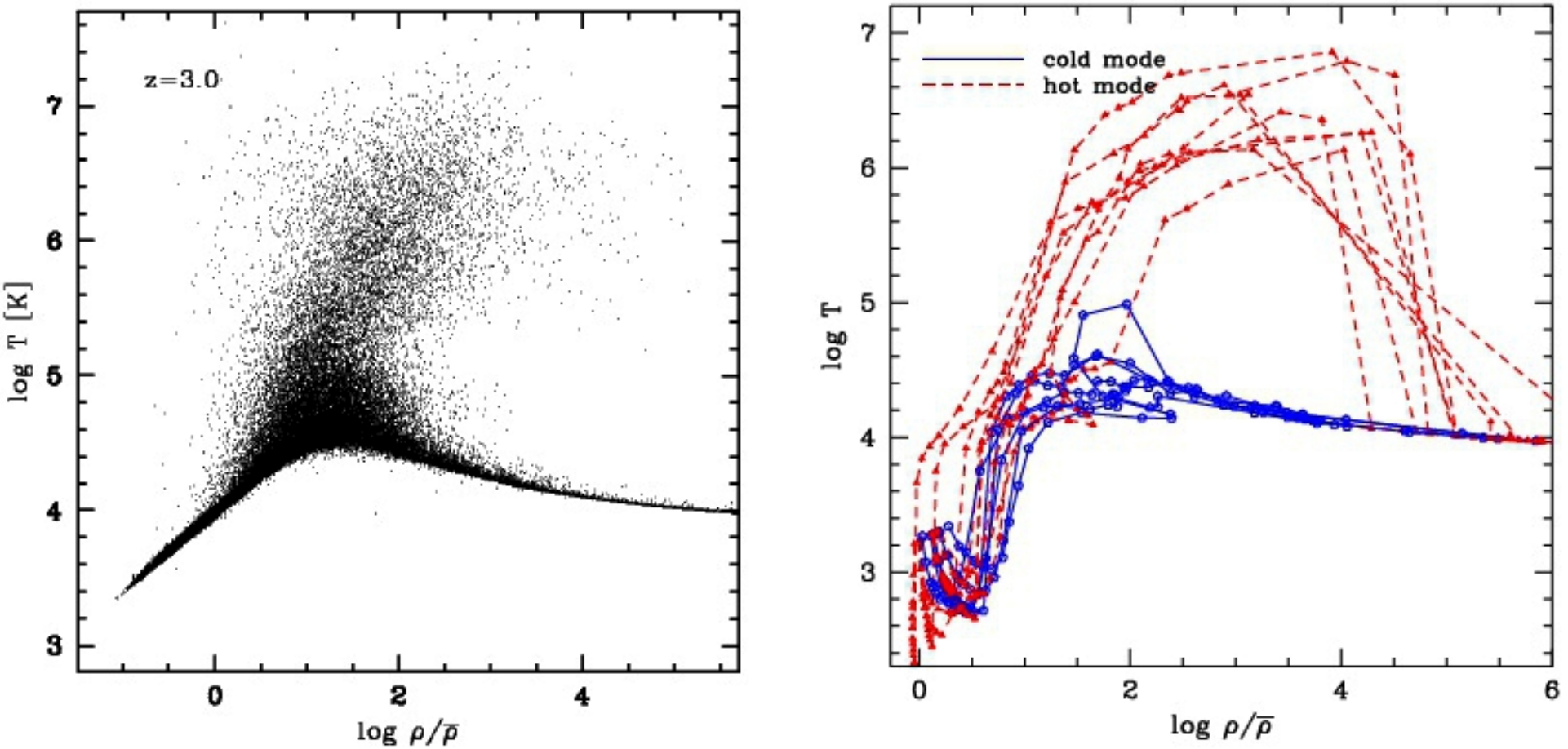

Figure 1. *Left*: Distribution of gas particles in the $\rho - T$ plane at $z = 3$, in the L22/128 simulation. One can easily identify three major phases: low density, low temperature gas in the photoionized IGM, shock heated overdense gas, and high density, radiatively cooled gas within galaxies. *Right*: Trajectories of 15 particles that accreted onto galaxies shortly before $z = 3$, illustrating the "cold" (solid lines, circles) and "hot" (dashed lines, triangles) accretion modes. Hot mode particles are shock heated above $\sim 10^{5.5}$ K before cooling, while cold mode particles move directly from the diffuse IGM phase to the dense, galactic phase without ever heating above 10^5 K. Trajectories start at $z = 14.9$ and end at $z = 3$. Points mark the individual redshift outputs, which have typical time separations of 0.05-0.1 Gyr.

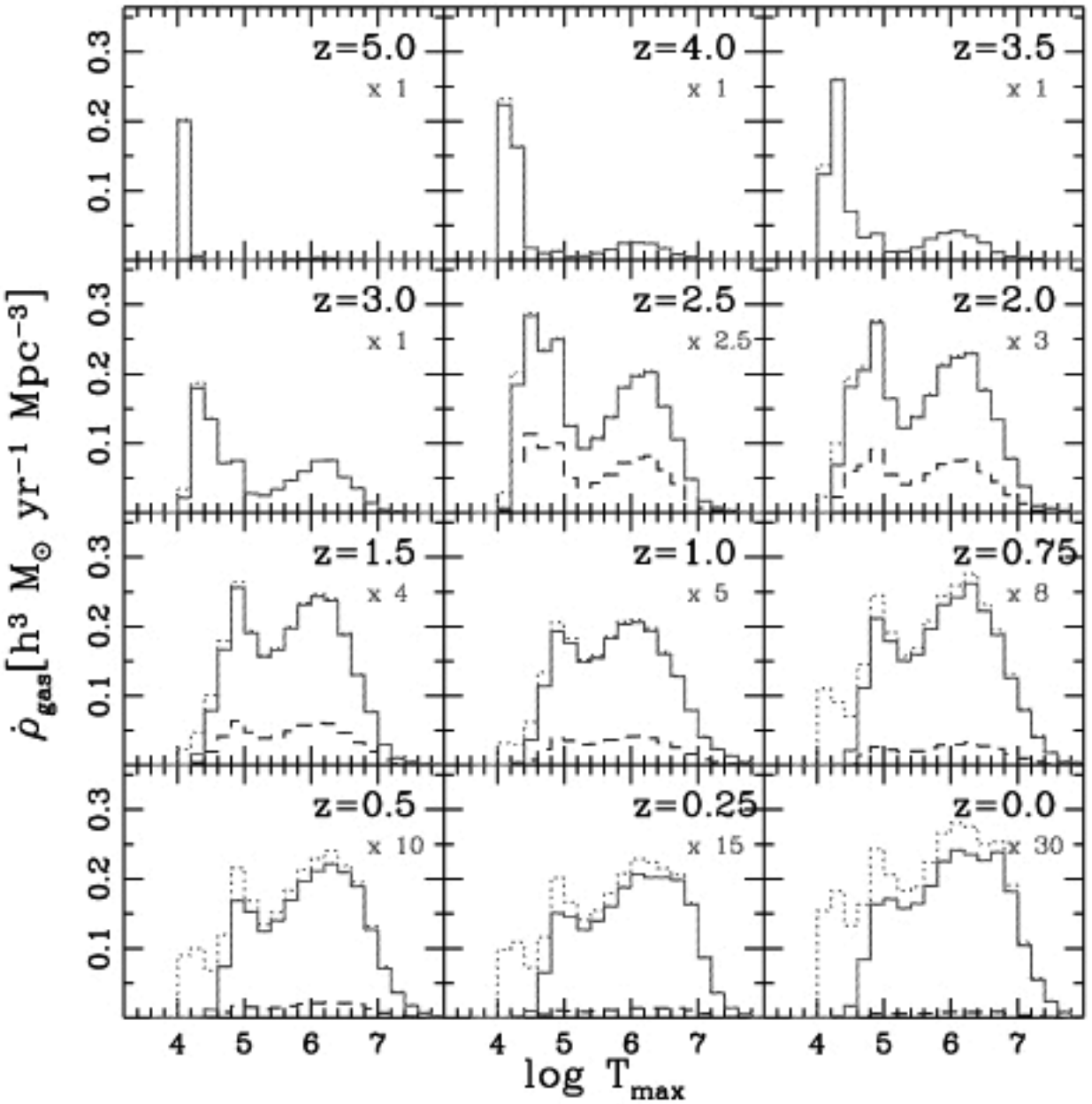

Figure 2. Distribution of maximum temperatures of gas accreting on to galaxies. For each particle that was smoothly accreted on to a resolved galaxy between the previous output and the plotted redshift, we trace back its history to determine the maximum temperature it had at any previous time. Dashed histograms show this distribution in units of $h^3\ M_\odot\ yr^{-1}\ Mpc^{-3}$ (comoving) per 0.2-dex bin of $\log T_{max}$. Solid histograms have the same shape but are multiplied by an arbitrary constant (as indicated in the panel) to improve visibility. Dotted histograms show the effect of including accreted stars in the calculation.

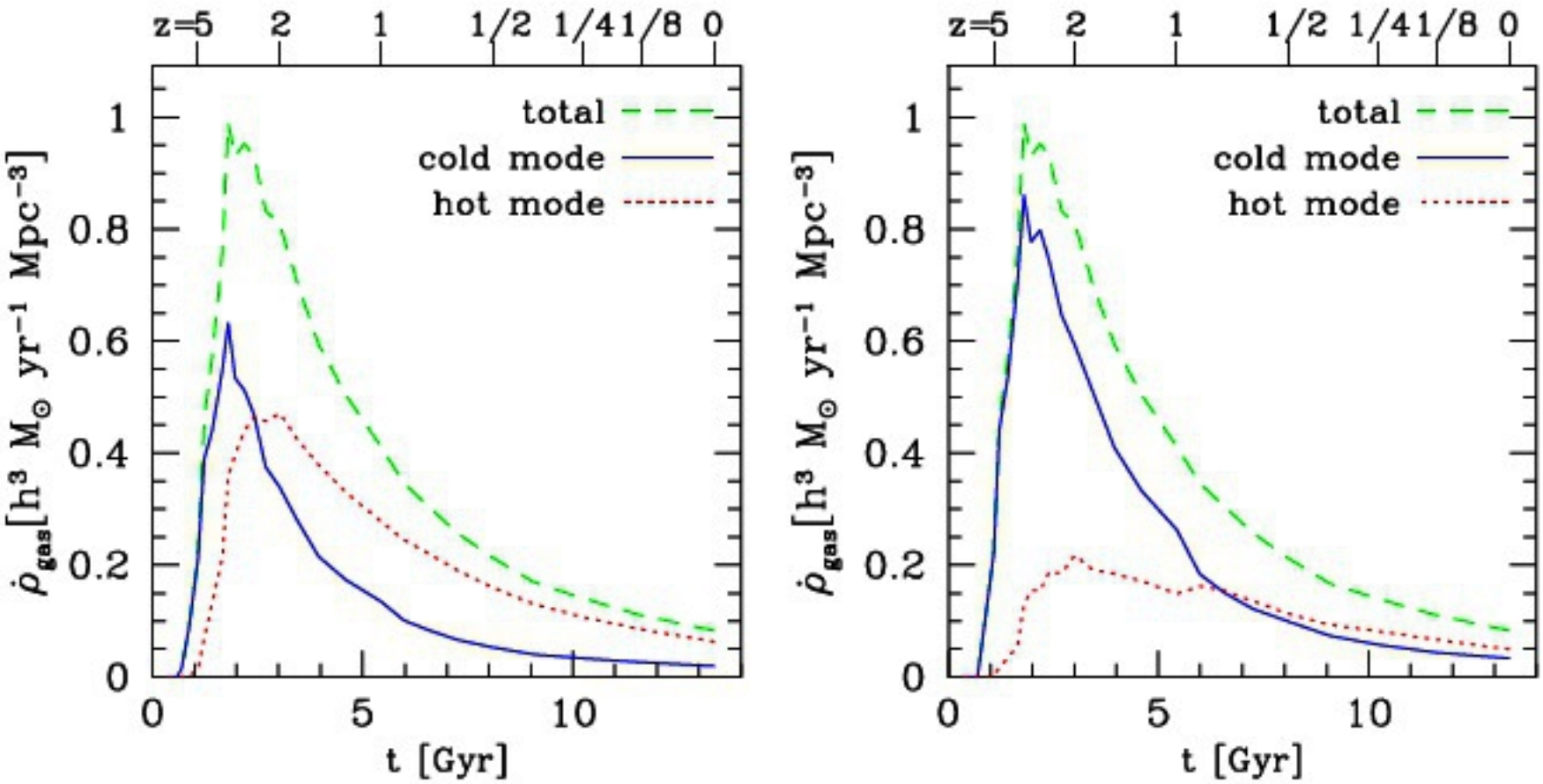

Figure 4. Redshift history of the total smooth gas accretion rate (dashed line), and the rates in cold mode and hot mode (solid and dotted lines, respectively). In the left panel, the division between hot and cold modes is at $T_{\rm max} = 2.5 \times 10^5$ K, while in the right panel it is at $T_{\rm max}/T_{\rm vir} = 1$.

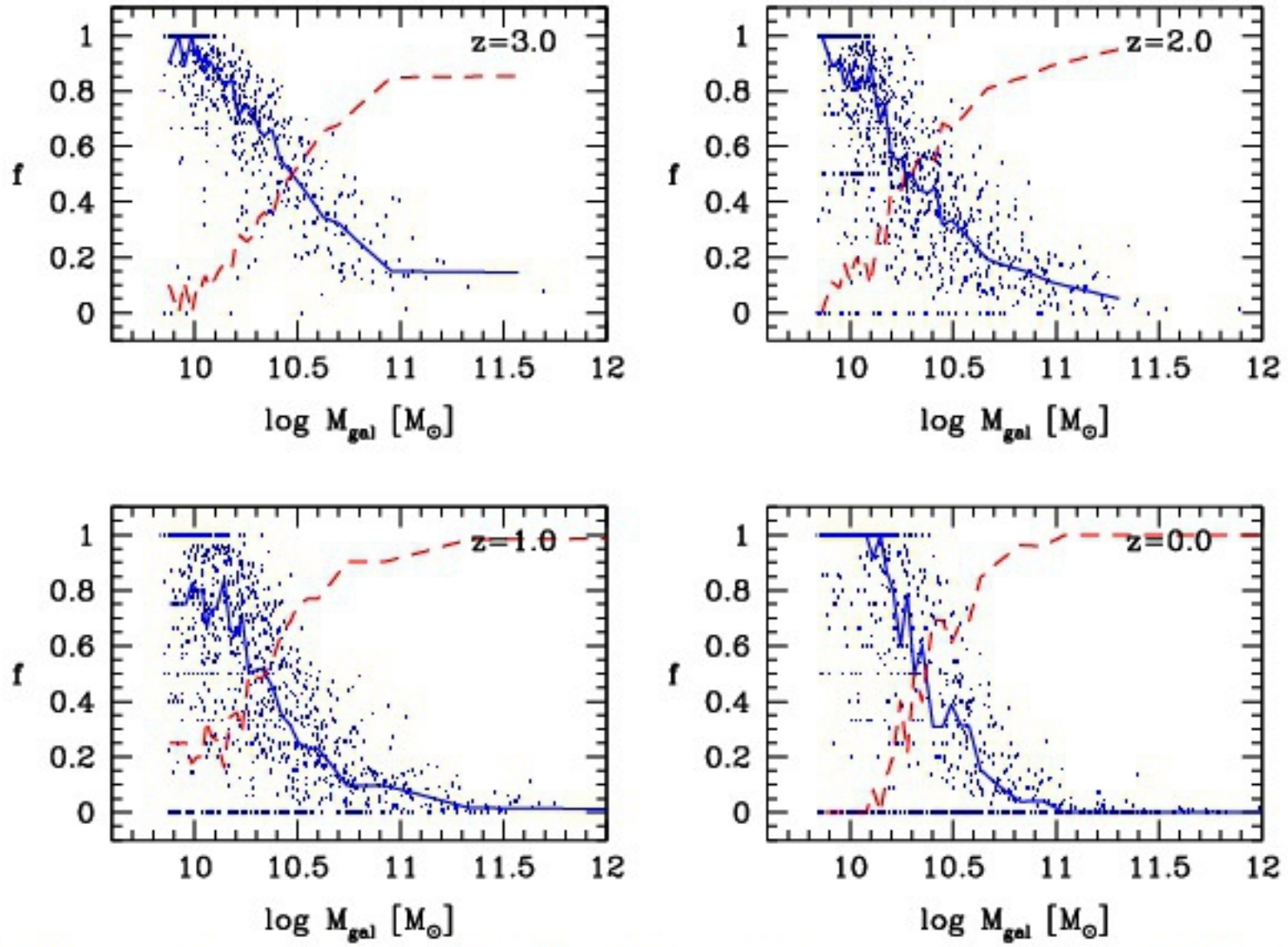

Figure 5. The cold accretion fraction as a function of galaxy baryonic mass (cold gas + stars), at $z = 3$, 2, 1, and 0. Points show the cold fractions of individual galaxies, and solid lines show the median values in bins of baryonic mass. Dashed lines show the median hot fraction; solid and dashed curves sum to one by definition.

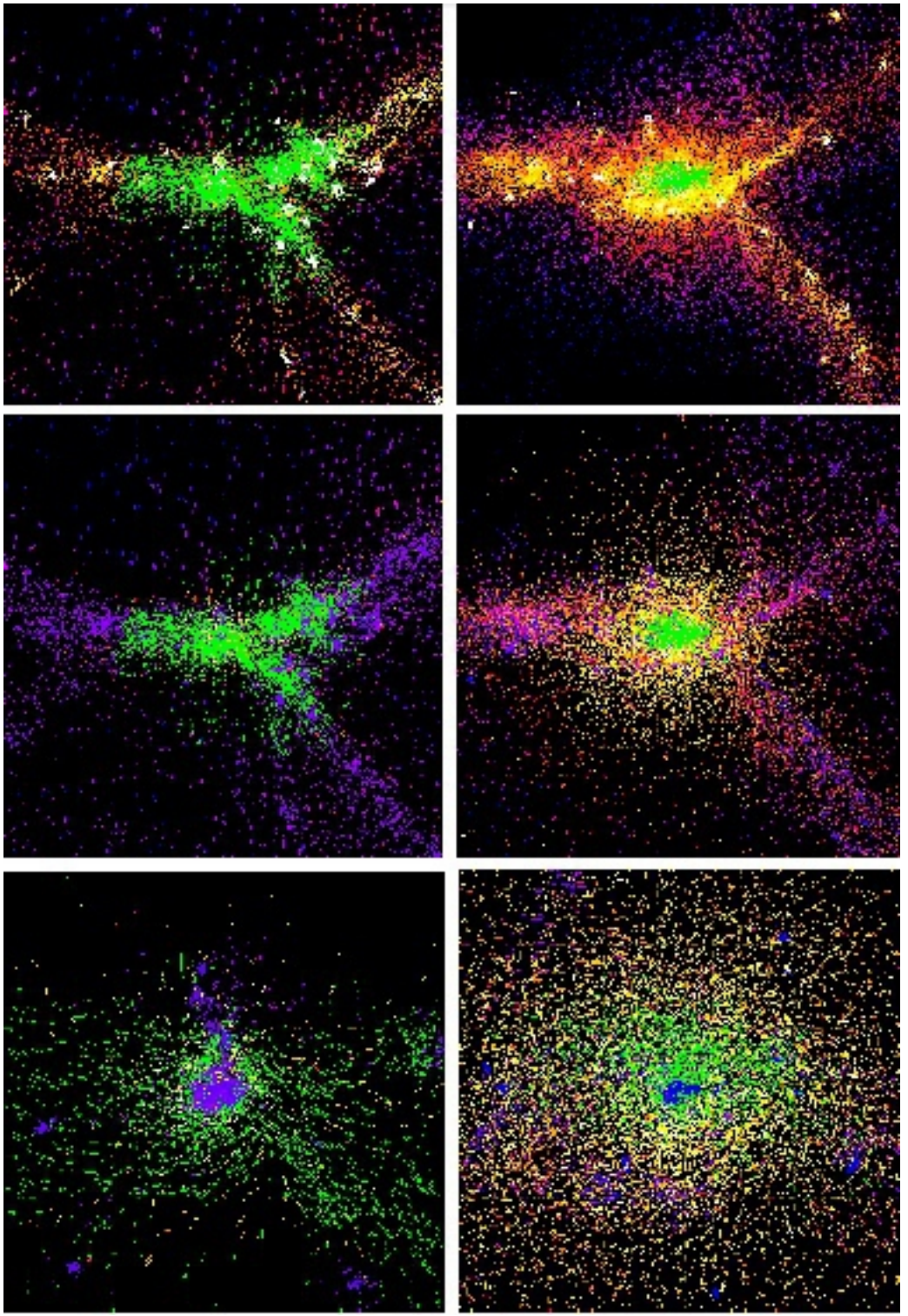

Left: galaxy with mass ~10^{10} M_{sun}

Right: galaxy with mass ~10^{11} M_{sun}

Left: Green represents particles which will be accreted in the cold mode in a few hundred million years.

Right: Green represents particles which will be accreted in the hot mode in a few hundred million years.

Bottom panel is a zoom.

LESSON: Cold mode accretion occurs Along filaments, hot mode accretion is spherical

CG fluid, especially "SPH" fluid (smoothed particle hydrodynamics), suffers from inaccurate physics at the microscopic level, at the scale of individual particles making up the fluid. Even when simulating with very large particle numbers, this becomes a major problem wherever the fluid becomes splashy since it forms thin sheets and strings -- or rather, it should form thin sheets and strings, like we see in real water.

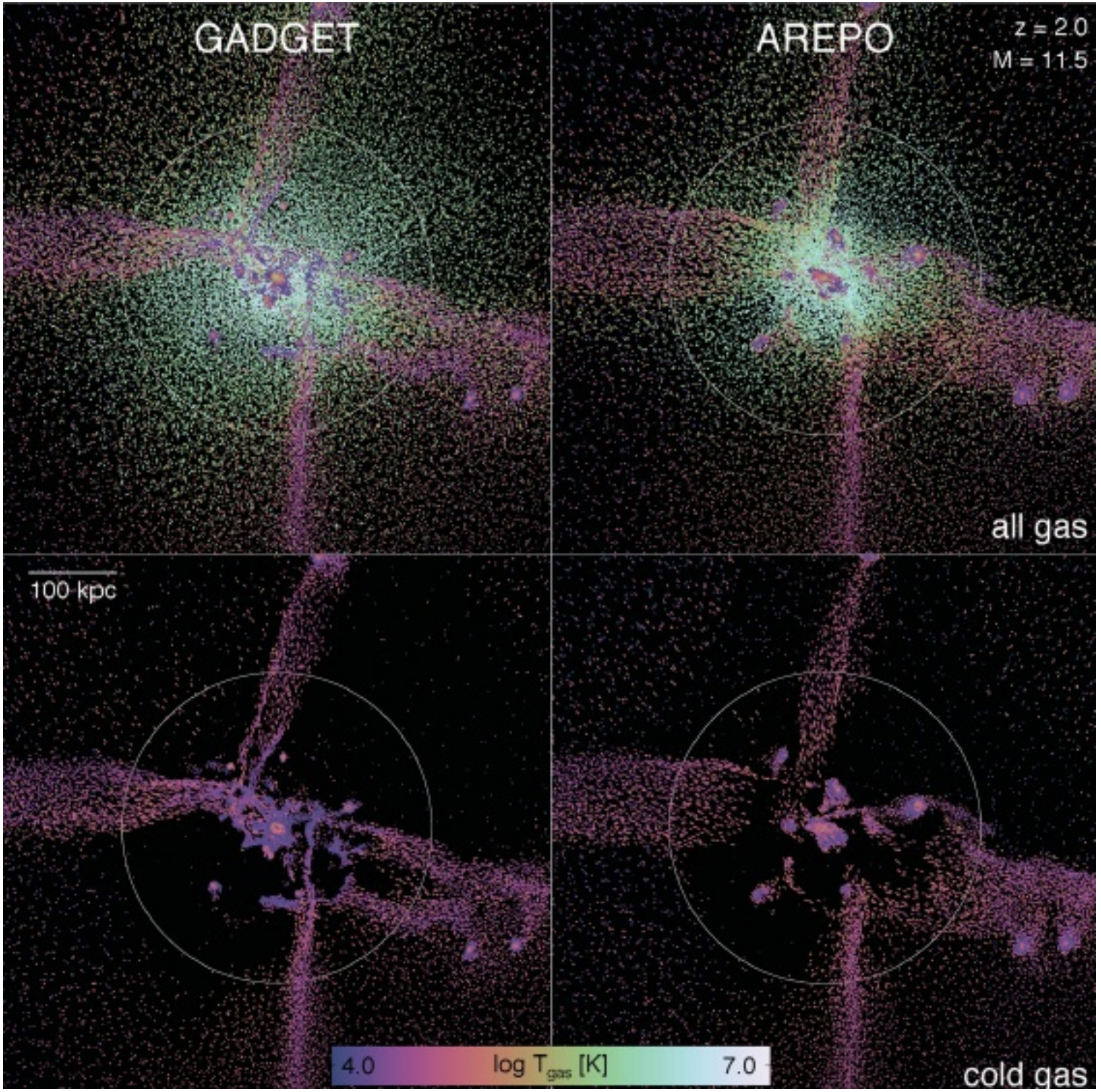
GADGET
AREPO
z = 2.0
M = 11.5
all gas
100 kpc
4.0
log T_gas [K]
7.0
cold gas

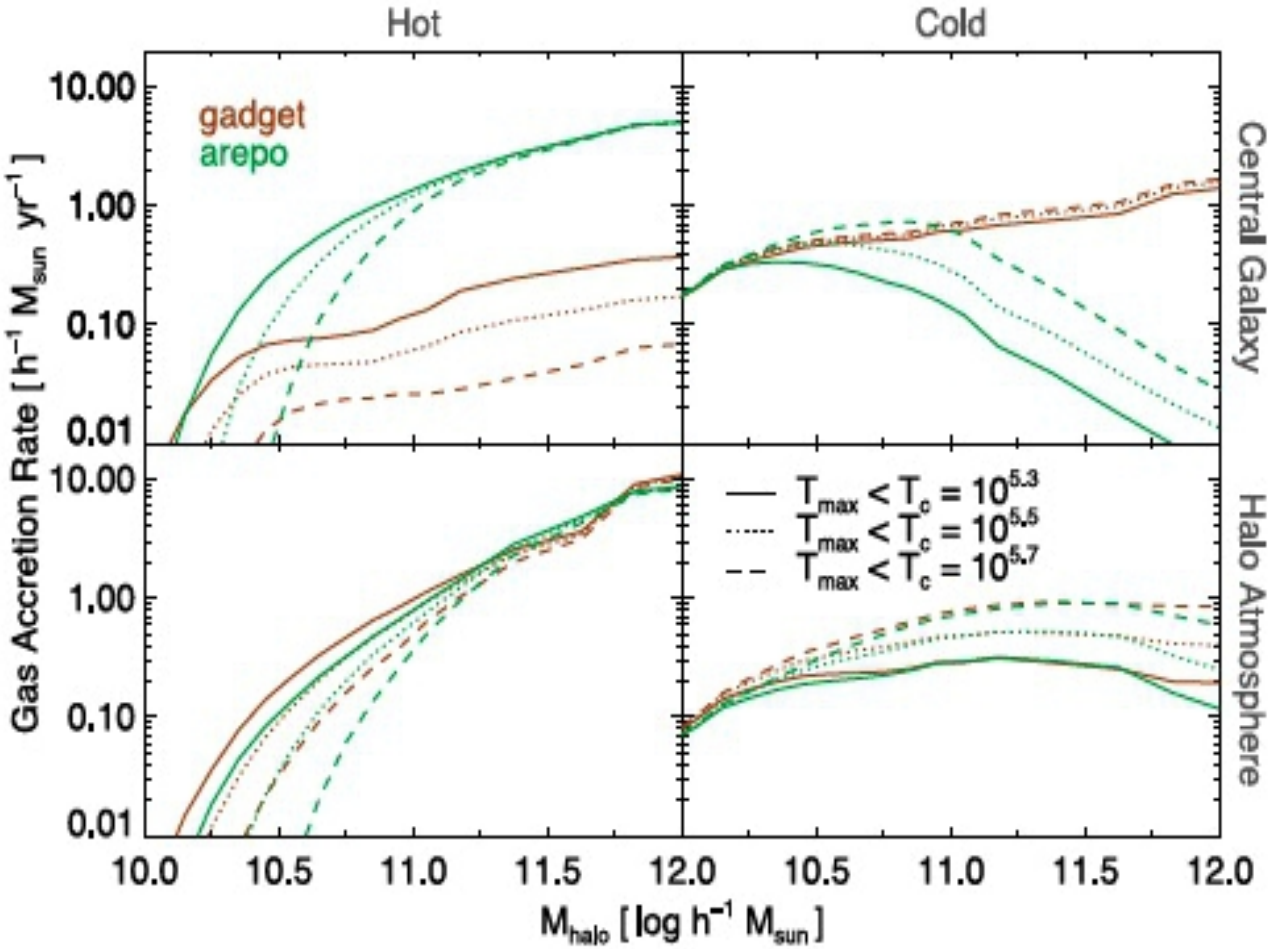

Figure 3. Gas accretion rate on to galaxies (top panels) and haloes (bottom panels). In all four panels, we define the cold mode as requiring T_{max} be less than a constant value T_c, as listed, demonstrating the sensitivity of the derived rates to the method of measuring the cold versus hot mode.

QSO absorption line spectroscopy as a tool for probing the gas around and between galaxies

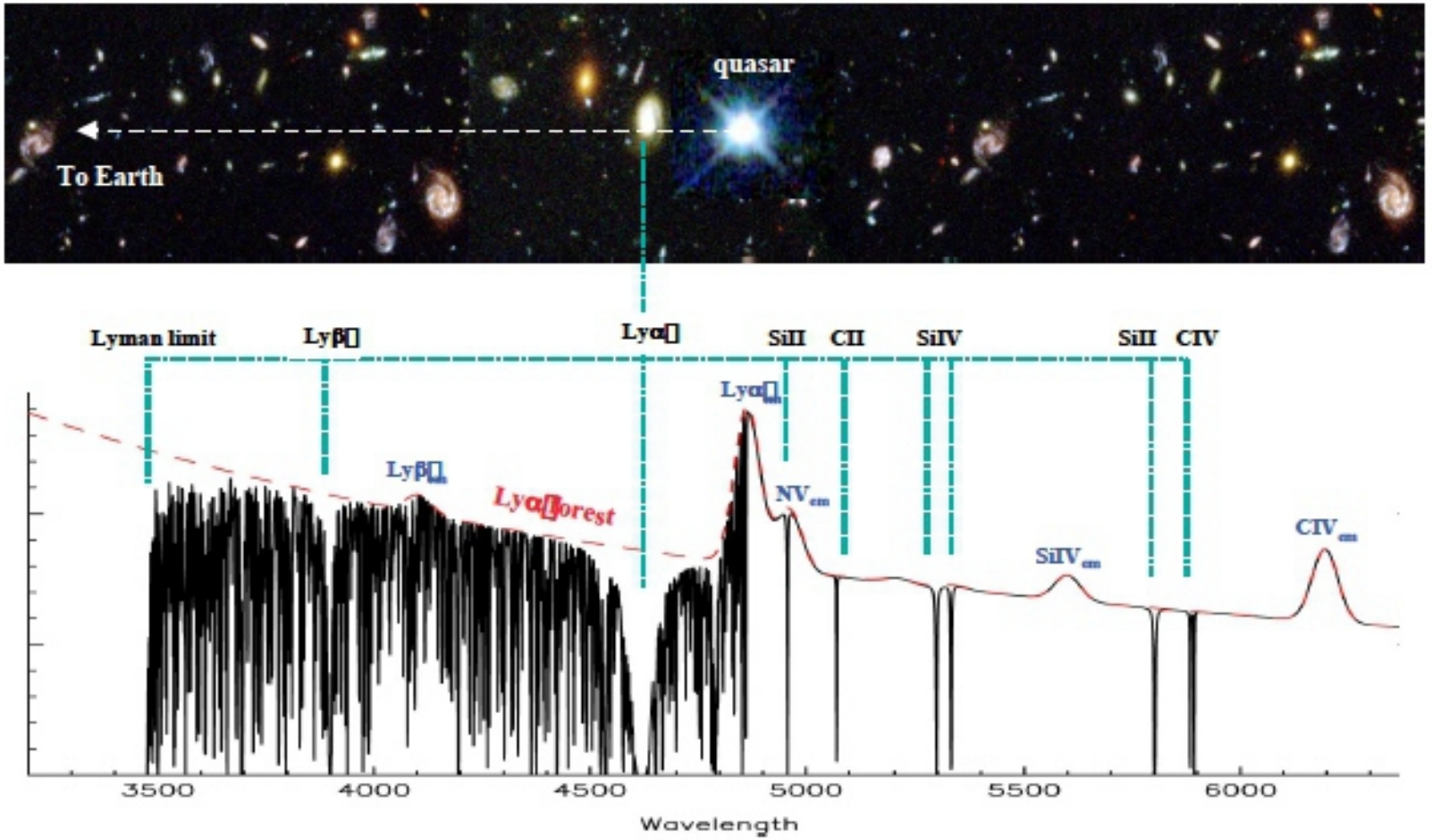

Figure 9.3: The spectra of distant QSOs bear the imprint of intervening gas—within galaxies and in the intergalactic medium—in the form of a rich variety of absorption lines (Figure courtesy of J. K. Webb).

QSOs (the active nuclei of distant galaxies) are some of the most luminous objects in the universe and can therefore be observed out to the largest distances (highest redshifts). Any galaxy or intergalactic cloud which by chance happens to lie between the QSO and us leaves its signature on the spectrum of the QSO in the form of absorption lines.

1) The QSO intrinsic spectrum consists of a power-law continuum, Typically $F \sim \lambda^{-1}$, and broad (several thousand km/s) emission lines. Both are produced close to the 'central engine', by gas close to the central super-massive black hole.

2) The strongest emission line is the first line in the Lyman series of neutral hydrogen, Lyman , corresponding to an electronic transition from the first excited level to the ground state .

3)Superposed on the intrinsic QSO spectrum are many narrow absorption lines, which are the focus of QSO absorption line spectroscopy.

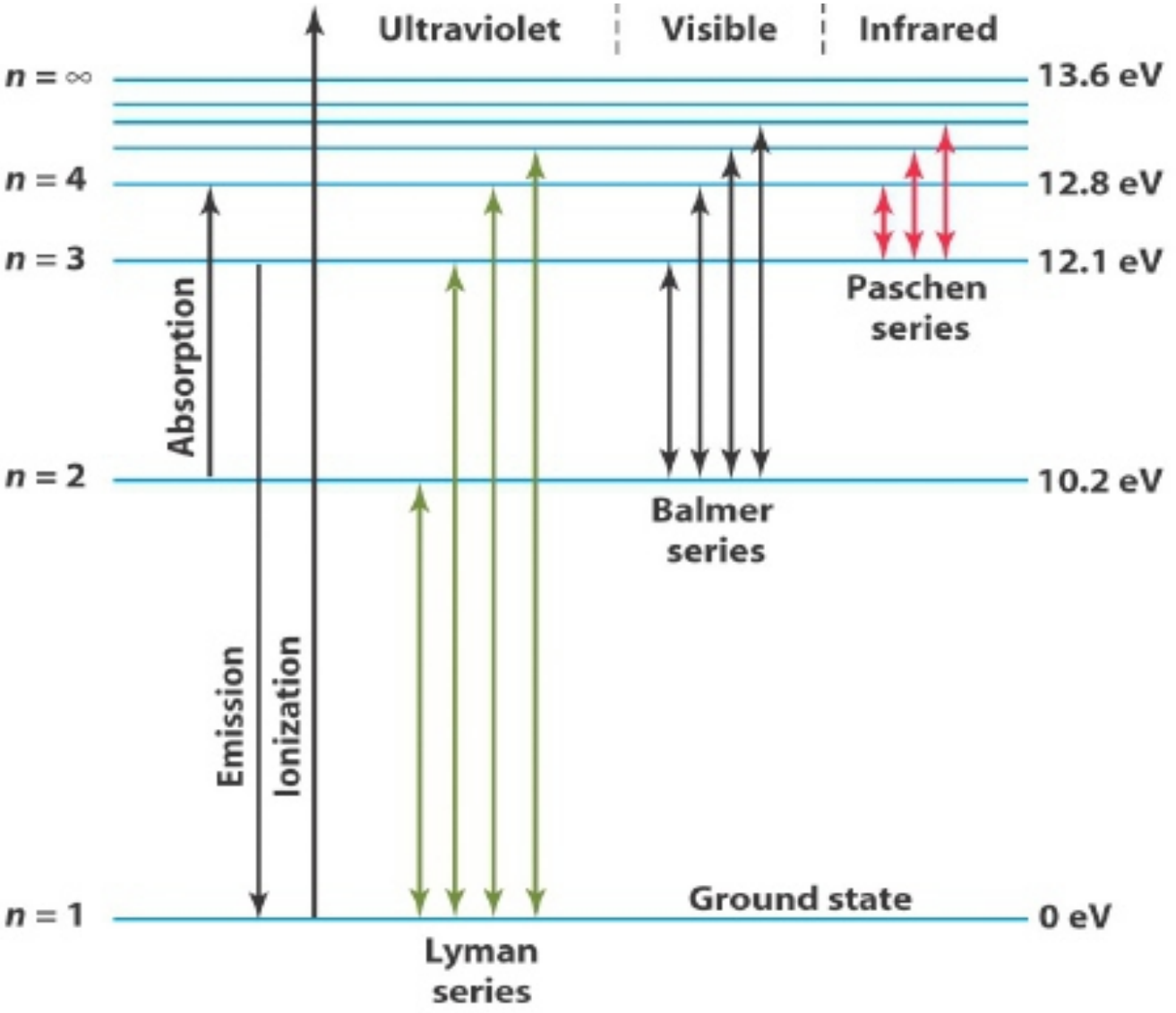

Figure 9.6: Schematic representation of the energy levels of the hydrogen atom.

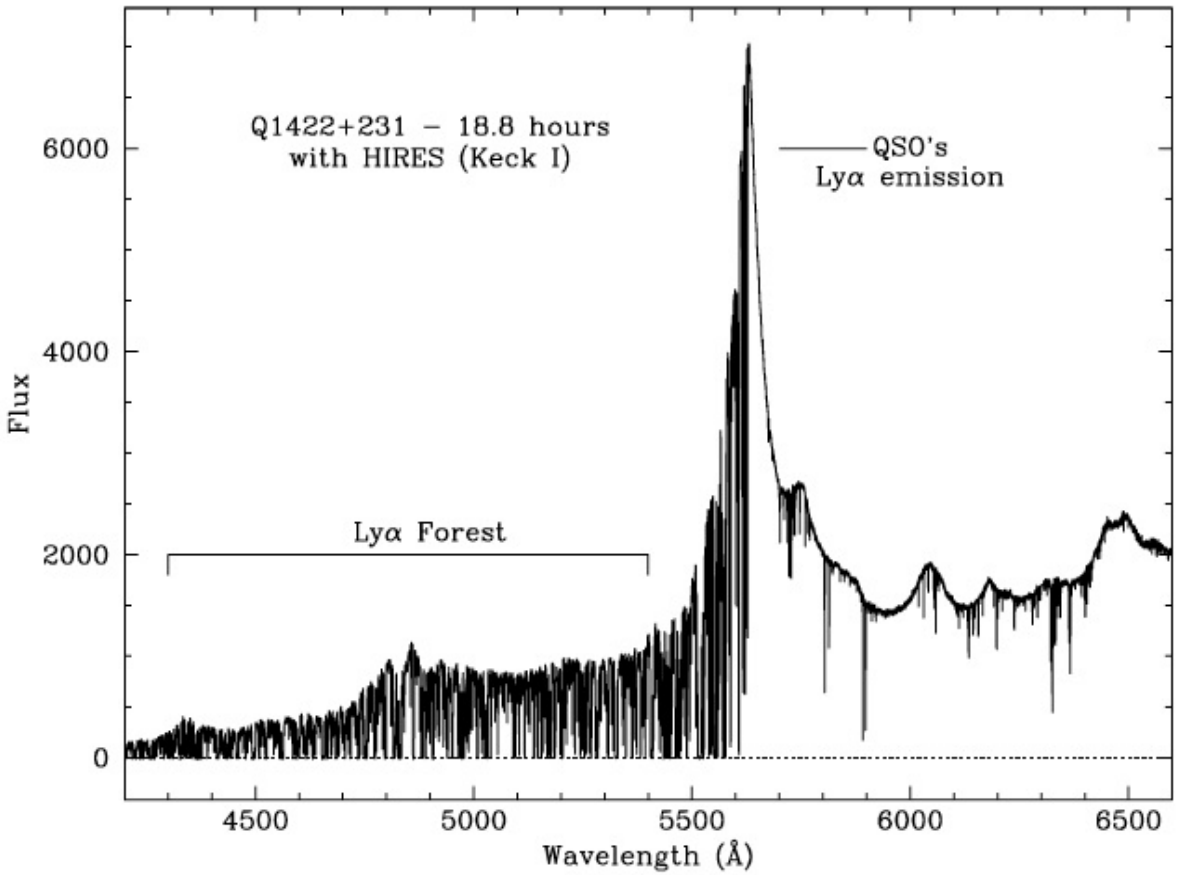

At shorter wavelengths than Lyα: single Ly lines arising in clouds where the column density of gas is too low to produce metal lines, the Lyman α forest.

At longer wavelengths than Lyα: the strongest resonance lines of the most abundant astrophysical elements (e.g. O **I**, C **II**, C **IV**, Mg **II**, Si **II**, Fe **II**) in well defined redshift systems. These are the 'metal-line' systems

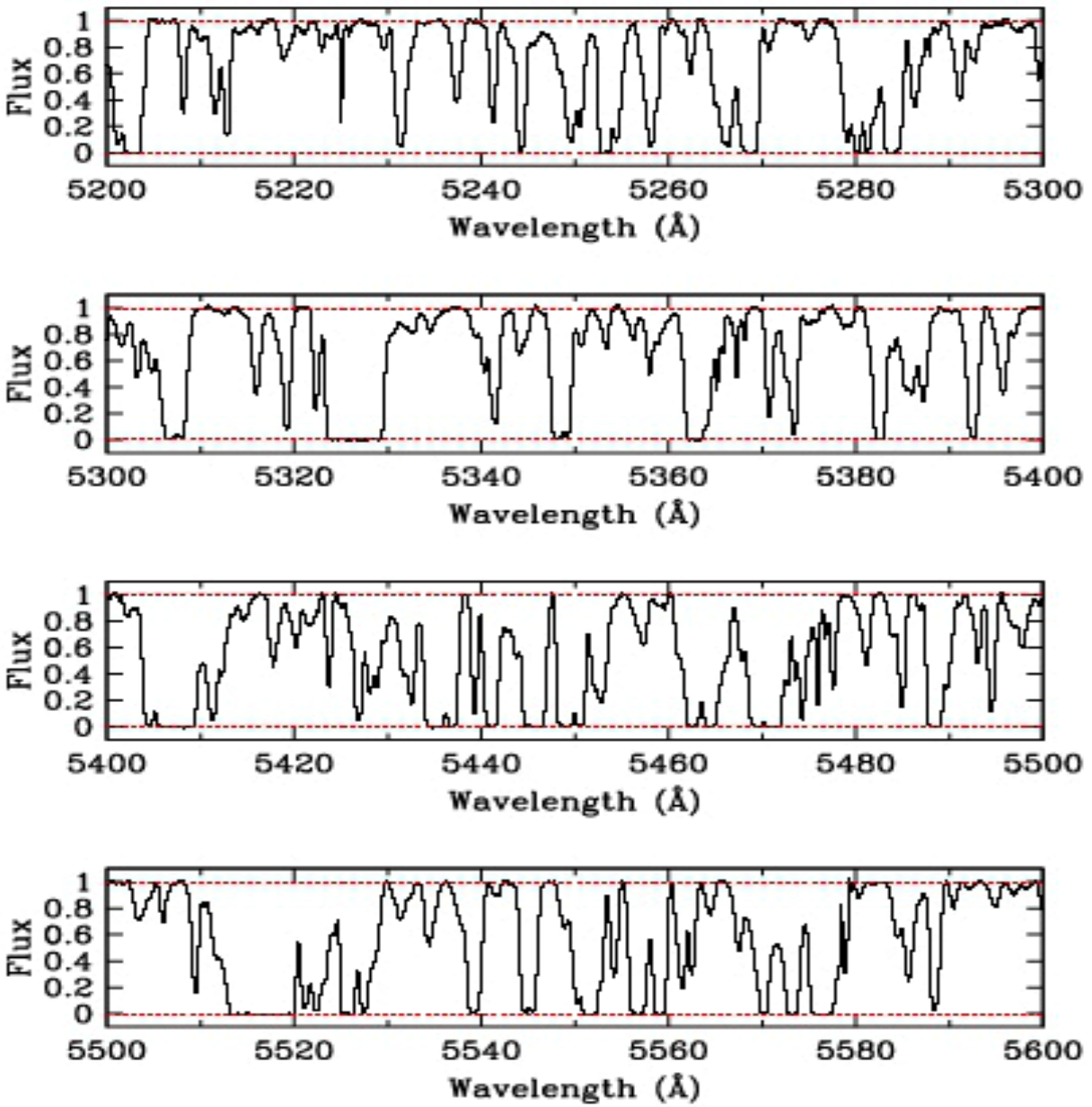

Figure 9.7: Expanded portion of the Lyα forest in the spectrum of the QSO Q1422+231 shown in Figure 9.4. The spectrum has been divided by the underlying QSO continuum;

Gunn-Peterson Optical Depth

Consider radiation emitted at frequency ν_e, lying blueward of Lyα by a source at redshift z_e. At a redshift z, such that $1+z=(1+z_e)\nu_\alpha/\nu_e$, the emitted photons pass through the local Lyα resonance as they propagate towards us through a smoothly distributed sea of neutral hydrogen atoms and are scattered off the line of sight with a cross-section (neglecting stimulated emission) of

$$\sigma[\nu_0(1+z)] = \frac{\pi e^2}{m_e c} f\ \phi[\nu_0(1+z)]$$

where f=0.4162 is the upward oscillator strength for the transition, φ is the line profile function (with normalization $\varphi\int\varphi(\nu)\,d\nu=1$), c is the speed of light and e and m_e are the electron charge and mass, respectively. The total optical depth for resonant scattering at the observed frequency is given by the line integral of this cross-section multiplied by the neutral hydrogen proper density $n_{HI}(z)$,

$$\tau_{GP} = \int_0^{z_e} \sigma[\nu_0(1+z)] n_{HI}(z) \frac{d\ell}{dz}\, dz$$

where $d\mathscr{l}/dz = cH_0^{-1}(1+z)^{-1}[\Omega_M(1+z)^3+\Omega_K(1+z)^2+\Omega_\Lambda]^{-1/2}$ is the proper line element in a Friedmann–Robertson–Walker metric and Ω_M, Ω_Λ and $\Omega_K=1-\Omega^M-\Omega_\Lambda$ are the matter, vacuum and curvature contributions to the present density parameter. As the scattering cross-section is sharply peaked around ν_α, we can write

$$\tau_{GP} = \int_0^{z_e} \sigma[\nu_0(1+z)] n_{HI}(z) \frac{d\ell}{dz}\, dz$$

In an Einstein–de Sitter ($\Omega_M=1$, $\Omega_\Lambda=0$) universe, this becomes

$$\tau_{GP}(z) = \frac{\pi e^2 f}{m_e H_0 \nu_\alpha} \frac{n_{HI}}{(1+z)^{3/2}} = 6.6\times 10^3 h^{-1} \frac{\Omega_b h^2}{0.019} \frac{n_{HI}}{\bar{n}_H} (1+z)^{3/2}.$$

Explanation of the Lyman α forest using cosmological simulations with gas dynamics

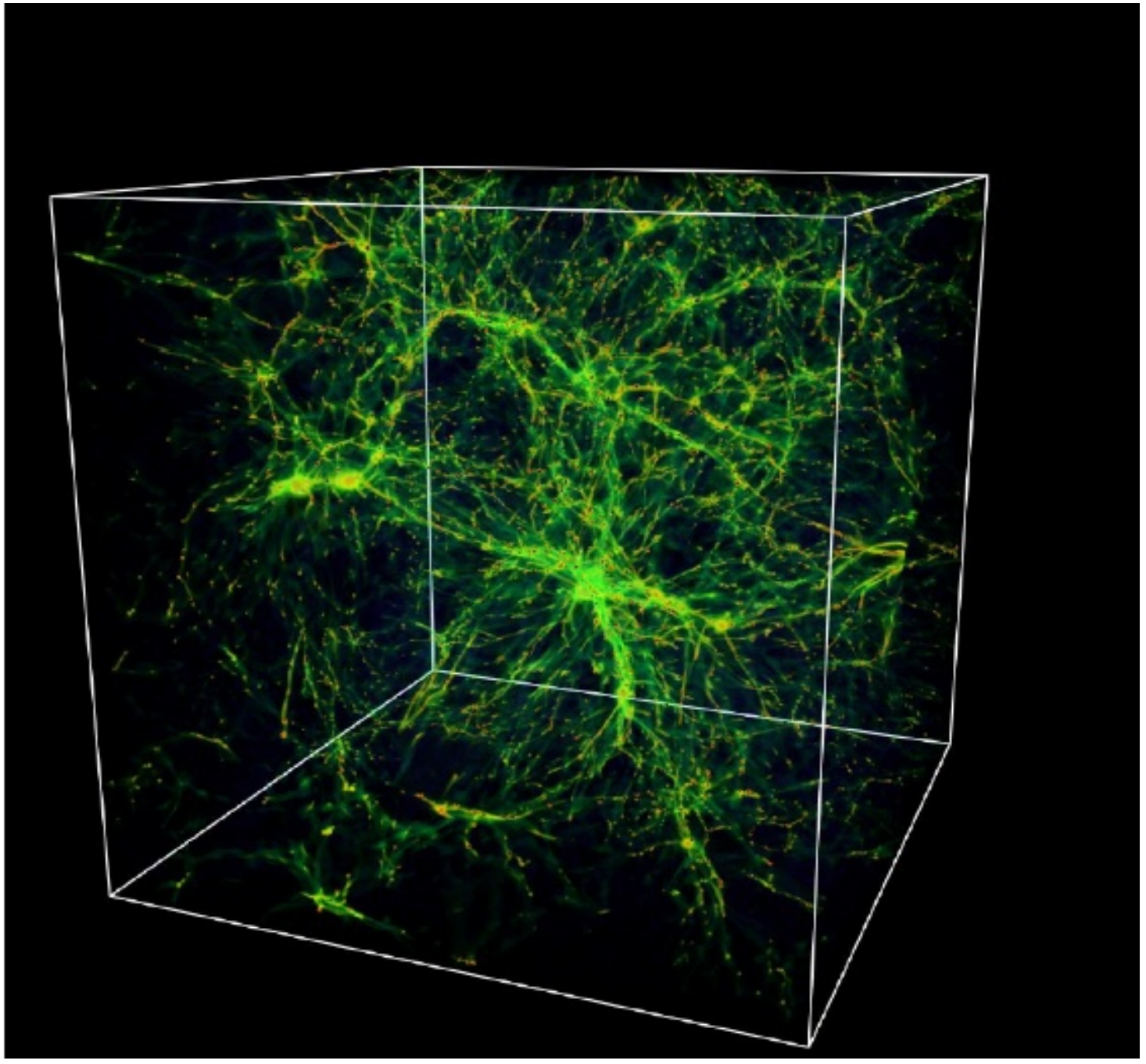

In the simulations, the optical depth to Lyman α scattering at a given projected position is calculated as:

$$\tau(V) = \tau_{\rm GP} \sum_i \{1 + \delta_{\rm H\,I}[x_i(V)]\} \frac{dx_i}{dV} .$$

Here, V is the component of the total velocity of the gas along the line of sight, with respect to an arbitrary origin; $x_i(V)$ are the set of all the positions along the line of sight where the gas moves with velocity V; and $\delta_{\rm H\,I}$ is the overdensity of neutral hydrogen.

This allows one to generate predicted spectra from the simulations.

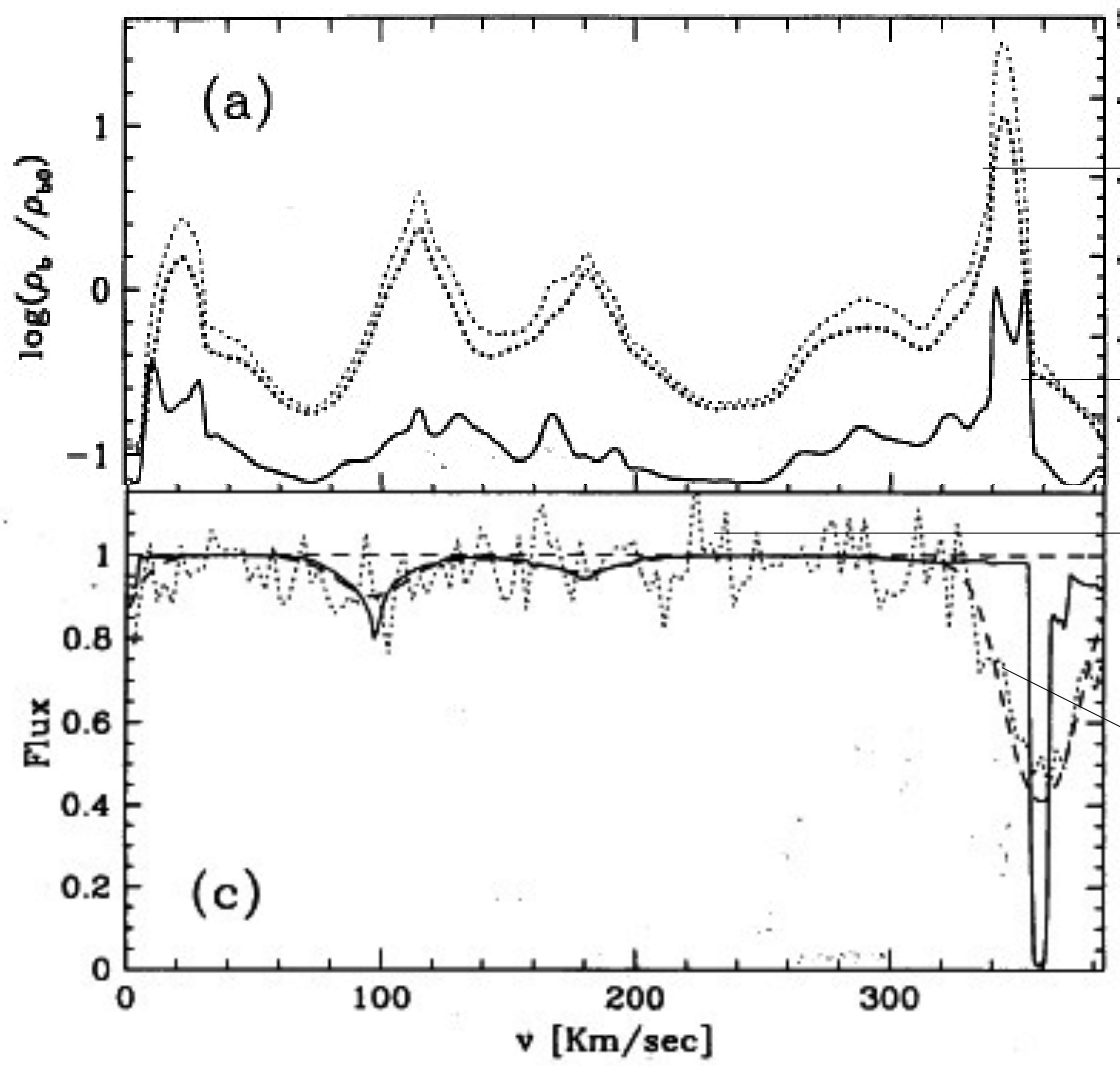
(a)
(c)
log(ρb /ρbo)
log(T) [K]
Flux
v [Km/sec]
density
temperature
Peculiar velocity
(deviation from
Hubble flow)
Predicted
spectrum

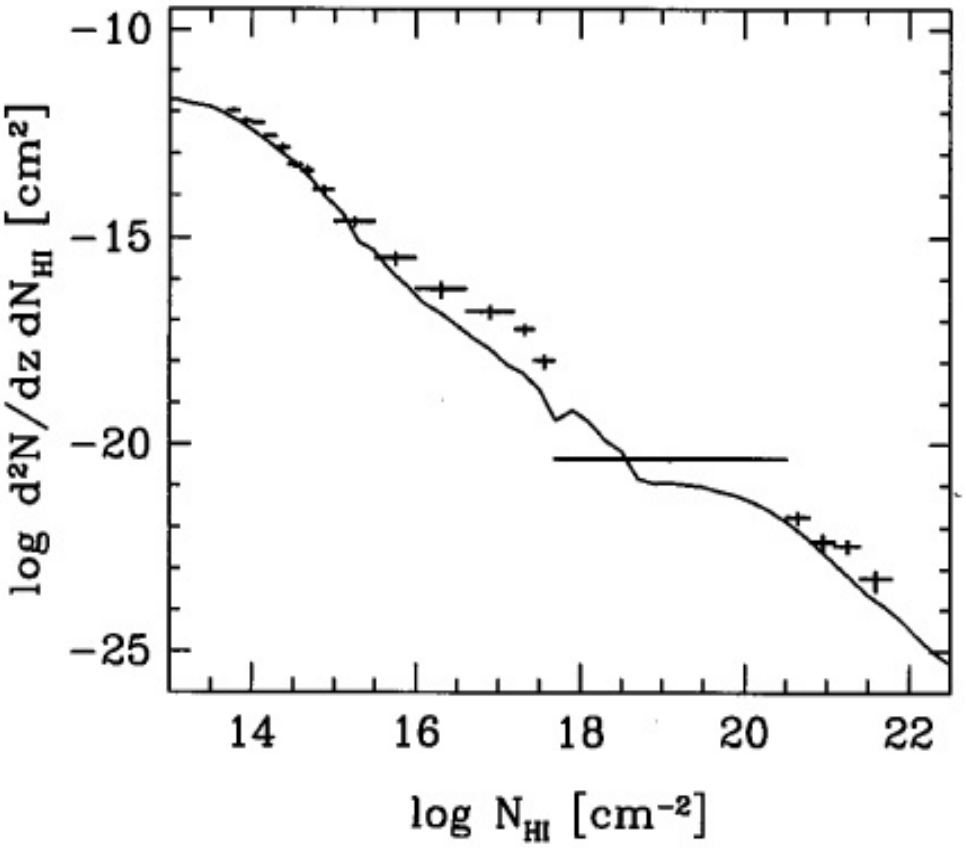

Comparison of neutral hydrogen column density distribution in Lyman alpha absorption lines in simulations and data.

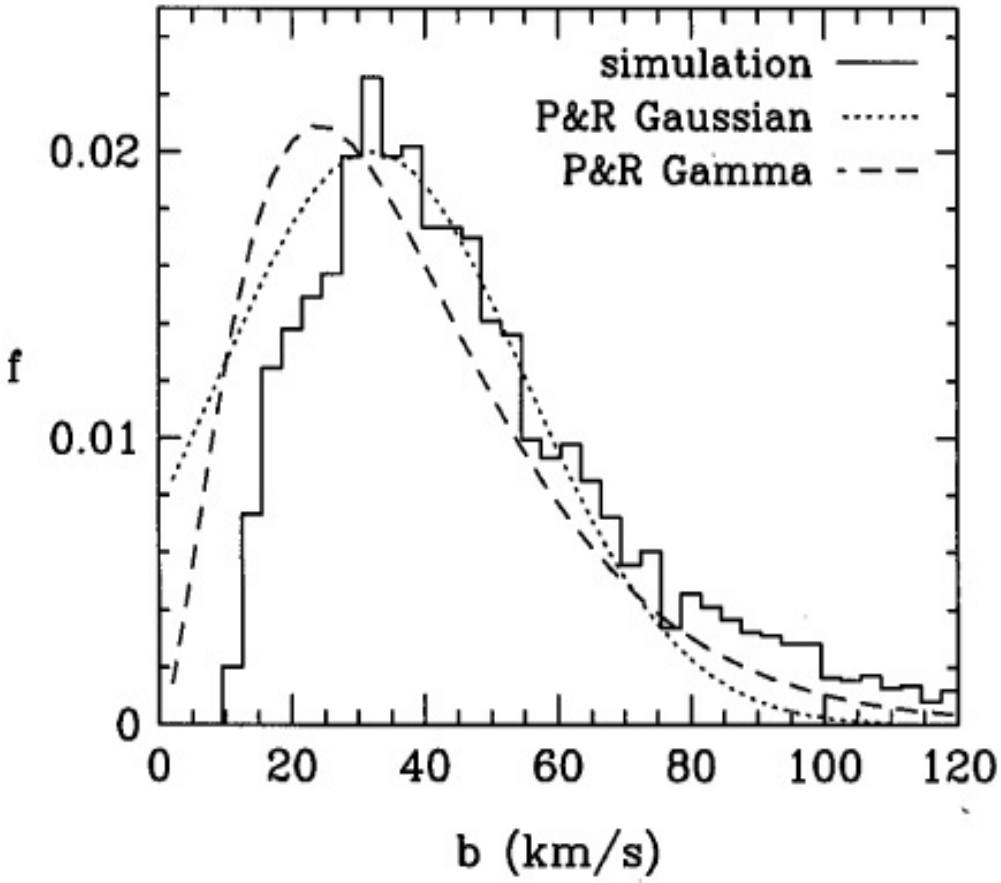

Comparison of widths of absorption lines in simulations and data.

Conclusion: Simulations can provide a very good description of the observations.

Hot Gas in Groups and Clusters

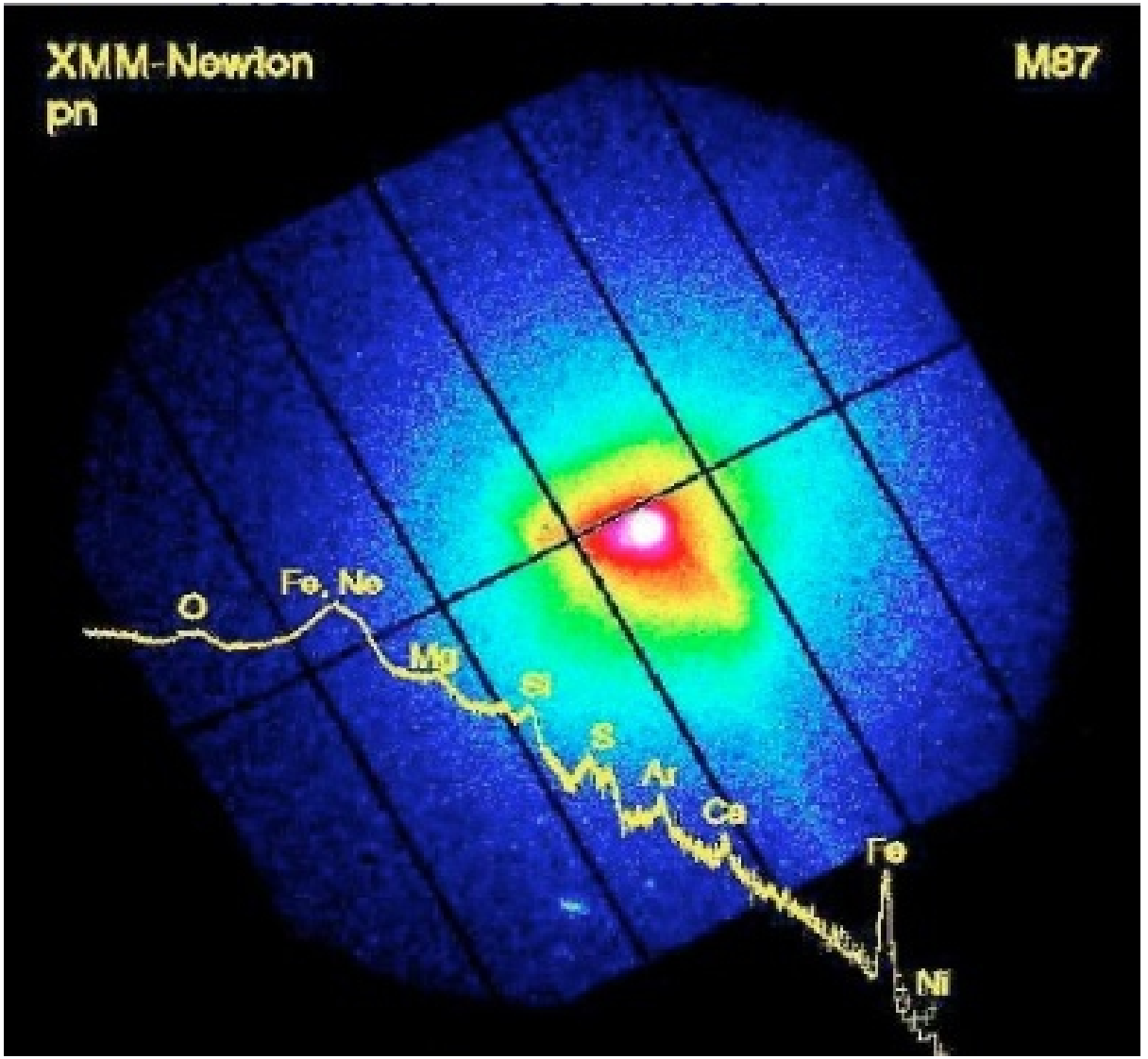

Analysis of X-ray Images

For given density and temperature distributions, $\rho_{\rm gas}(\mathbf{x})$ and $T(\mathbf{x})$, the bremsstrahlung emissivity can be calculated at each position $\mathbf{x} \equiv (r, \mathbf{R})$ in the cluster, where r is the radial coordinate along the line of sight, and $\mathbf{R}$ labels the position in the perpendicular plane. The X-ray surface brightness at a position $\mathbf{R}$ on the sky can then be obtained by integrating the emissivity along the line of sight:

$$S_{\rm X}(\mathbf{R}) = \frac{1}{4\pi} \int {\rm d}\nu w(\nu) \int {\rm d}r \frac{\varepsilon_{\rm ff}[r, \mathbf{R}; \nu(1+z)]}{(1+z)^3},$$

where $w(\nu)$ is a response function of the pass band, z is the redshift of the source, and $\varepsilon_{\rm ff} \propto \rho_{\rm gas}^2 T^{-0.5}$ is the (free-free) bremsstrahlung emissivity (see §A2.3). The surface brightness is usually averaged in circular annuli centered on the cluster center. The resulting distribution is then fit to some theoretical profile. If the cluster is spherically symmetric, the observed surface brightness profile provides a constraint on the combination of $\rho_{\rm gas}(r)$ and $T(r)$.

With X-ray Spectroscopy

, one can determine the temperature profile $T(r)$, and thus also the gas density profile $\rho_{\rm gas}(r)$. This can then be used to infer the total mass of the cluster from the hydrostatic equation (8.16).

A simple model commonly used to fit cluster X-ray data assumes that the cluster is an isothermal sphere whose total mass distribution is given by

$$\rho_{\rm m}(r) = \rho_{\rm m}(0)\left[1+(r/r_0)^2\right]^{-3/2},$$

where r_0 is a core radius. As we have seen in §8.2, this profile is valid only for the inner region ($r \lesssim 2r_0$) of an isothermal sphere. From Eq. (8.26) we see that the profile of the gas in hydrostatic equilibrium in such a cluster is

$$\rho_{\rm gas}(r) = \rho_{\rm gas}(0)\left[1+(r/r_0)^2\right]^{-3\beta/2},$$

where β is the ratio of the specific energies of the dark matter and the gas [see Eq. (8.27)]. The corresponding X-ray surface-brightness profile is then

$$S_{\rm X}(R) = S_0\left[1+\left(\frac{R}{r_0}\right)^2\right]^{-3\beta+1/2},$$

The Fe-L-Shell-Line Complex as a Thermometer

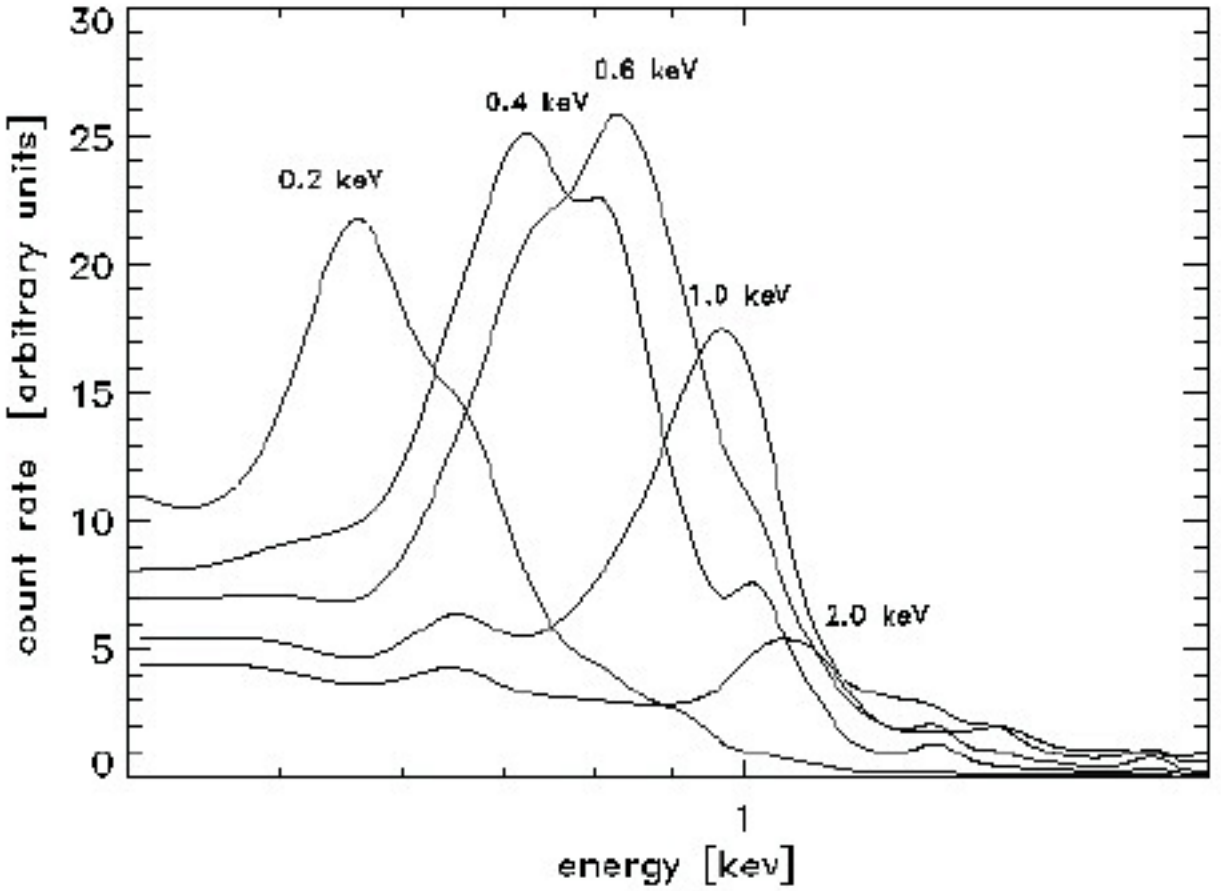

The iron l-shell line blend as a function of temperature

Determination of Cluster Mass Profiles from XMM-Newton Observations

Surface brightness and temperature profile of the massice cluster A1413 [Pratt & Arnaud 2002]

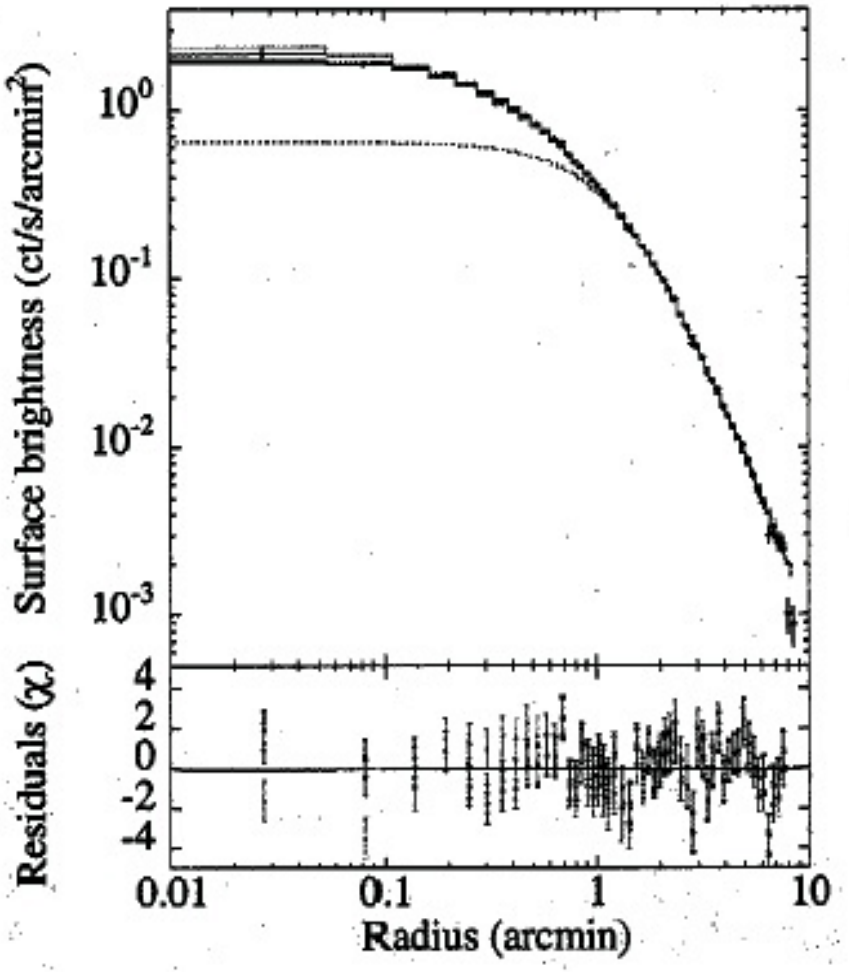

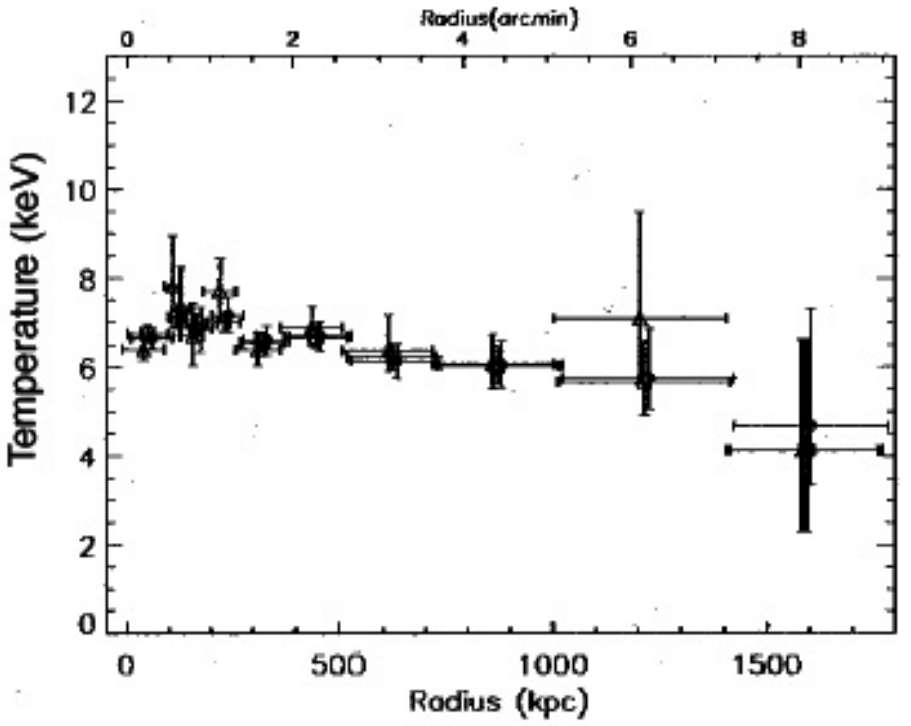

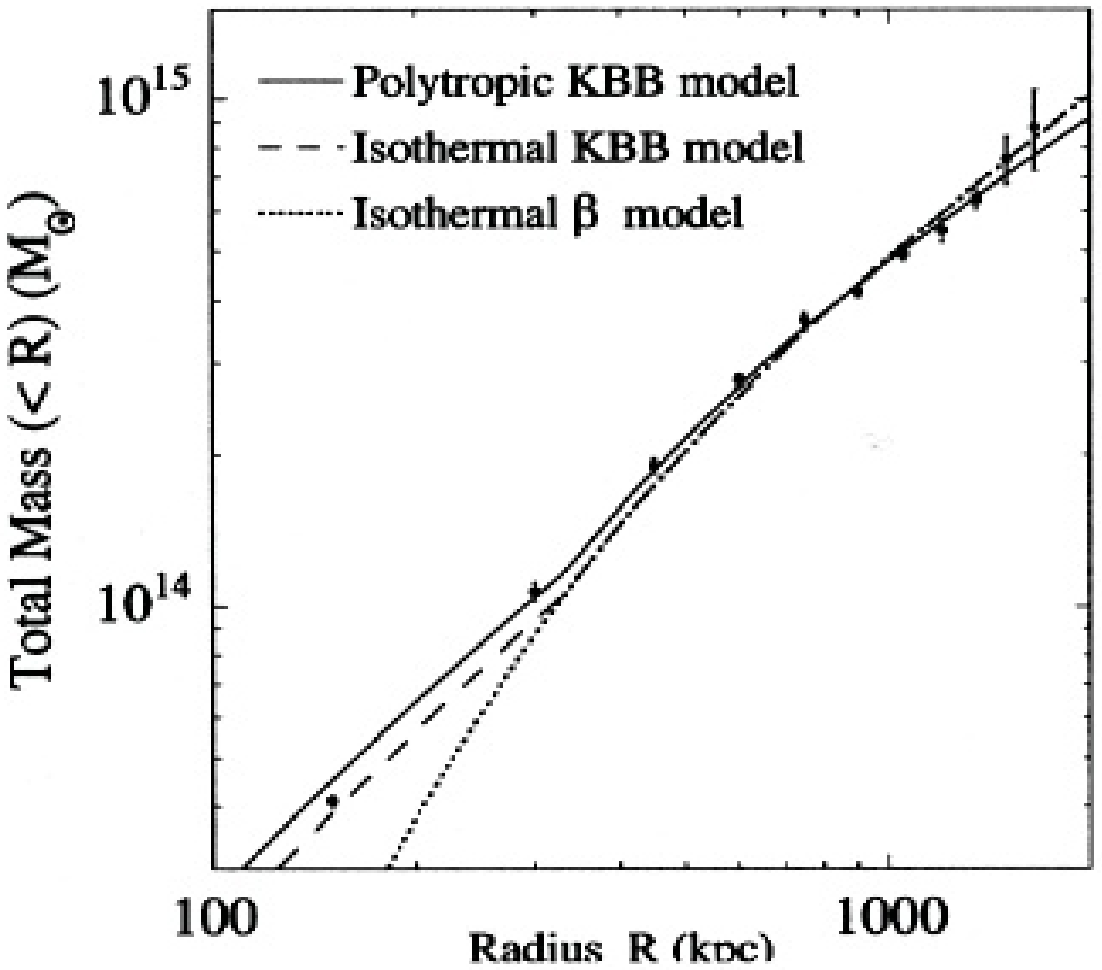

Cluster A1413

Gas Mass Fraction @ r_{500}

Data from Arnaud et al. 2007, Vikhlinin et al. 2006, Sun et al. 2008

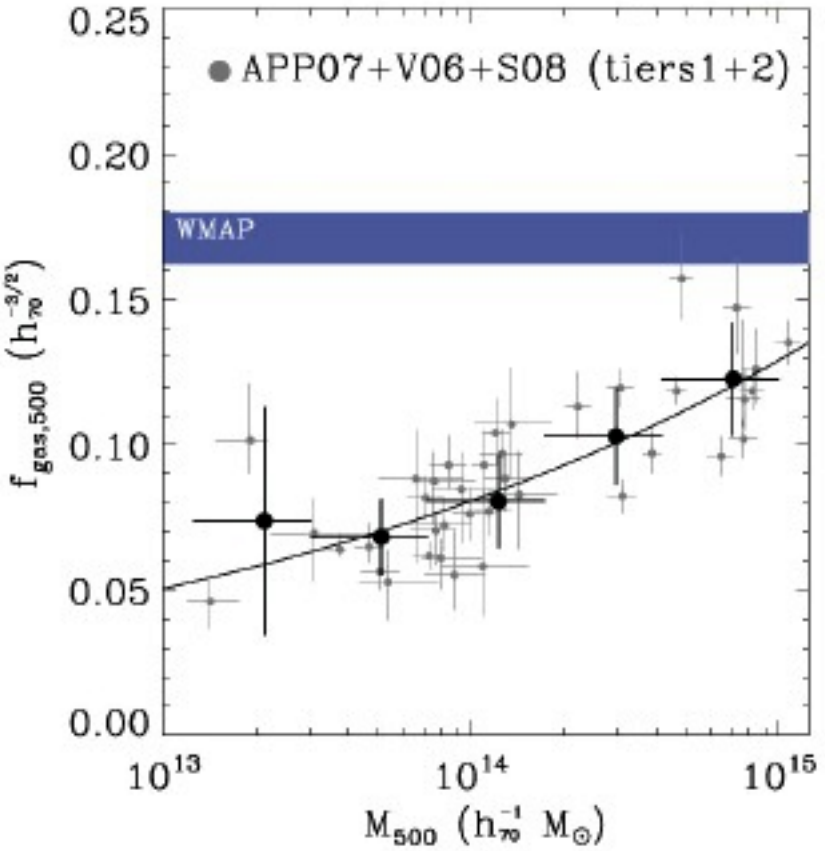

Data from the REXCESS sample

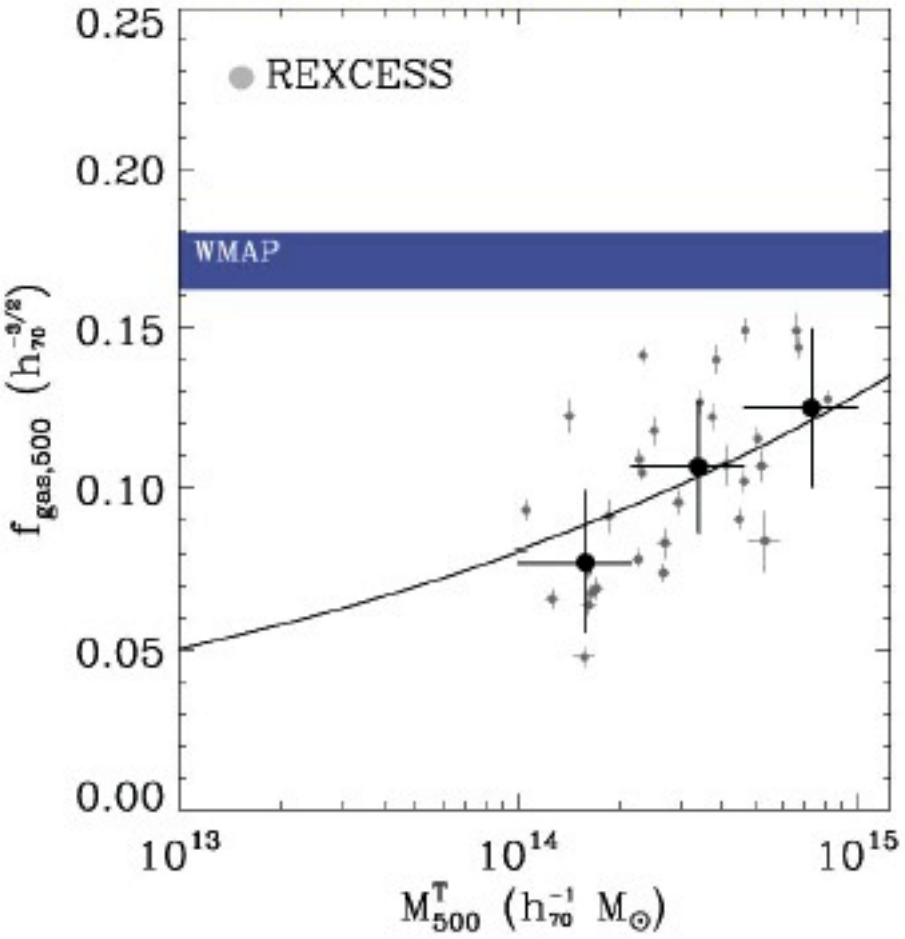

Small systems have a large gas mass deficiency – due to the more massive feedback effects

[Pratt et al. 2009a]

Cooling Flows

Since the hot gas is roughly in hydrostatic equilibrium within the gravitational potential of the cluster, its density in general increases towards the center. The cooling time typically becomes shorter at smaller cluster-centric radii. The densities and temperatures of the ICM inferred from X-ray data indicate that the cooling times in the central ~ 100kpc of most clusters are shorter than 10^{10} yr. Consequently, in the absence of a balancing heat source, a slow, subsonic inflow of gas is expected to develop in the central regions.Cooling reduces the temperature and thus the pressure of the gas. In order to support the weight of the overlying gas, the central gas has to increase its density, which it does by flowing inward.

A first order estimate of the mass deposition rate is simply made by taking the total gas mass calculated from the density profile and dividing that by the cooling time at the edge of the region. Inferred mass deposition rates reach 100-1000 Msun/year

A detailed Spectral Investigation of the „Cooling Flow" Region in M87

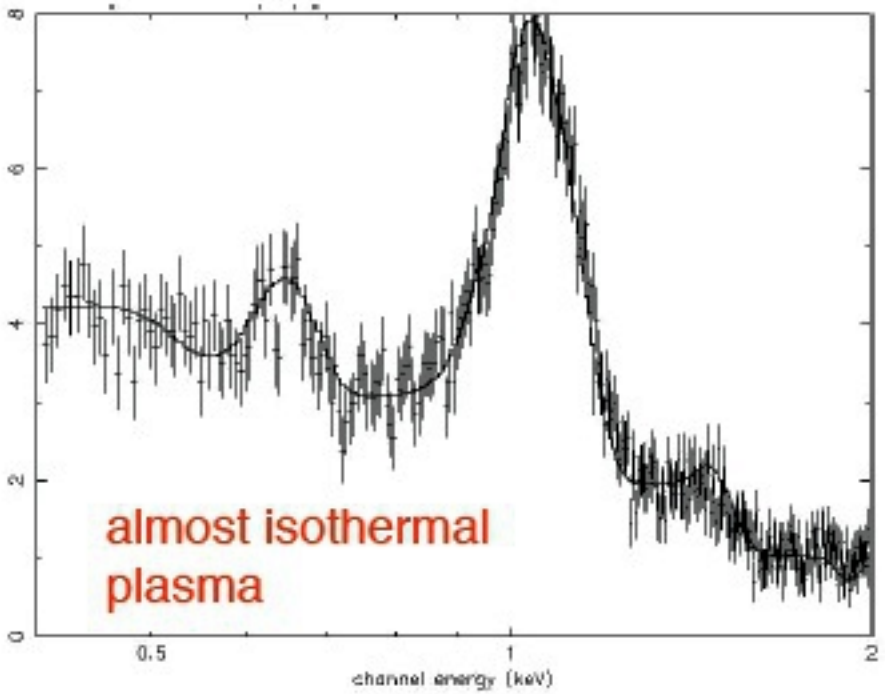

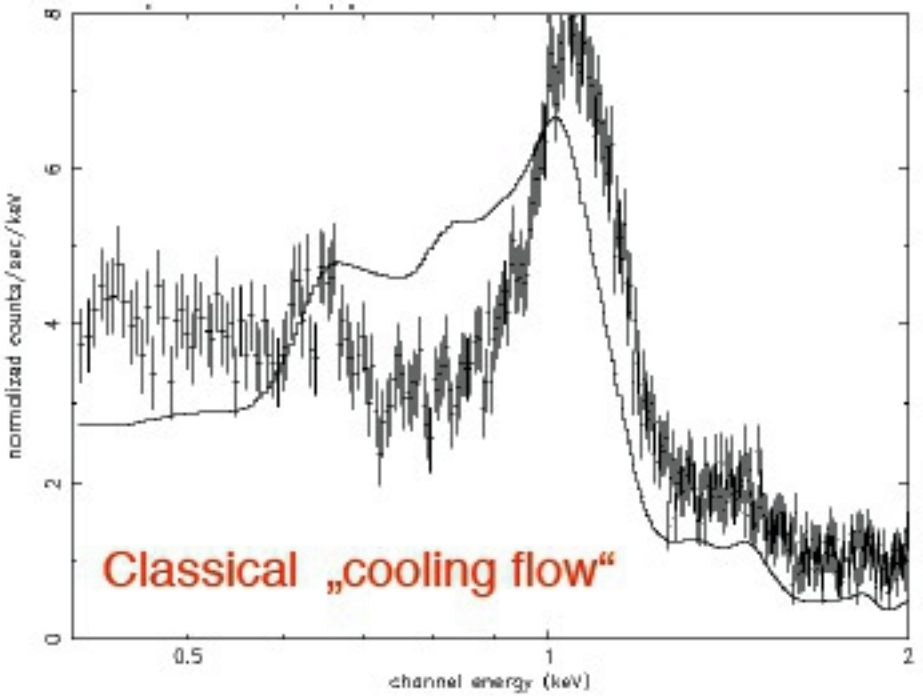

$N_H = 1.8\ 10^{20} cm^{-2}$ (fix)

$T_{high} = 2.0$ keV (fix)

$T_{low} = 1.44$ keV (free)

$\dot{M} = < 2.4\ M_{sun}/yr$

$N_H = 1.8\ 10^{20} cm^{-2}$ (fix)

$T_{high} = 2.0$ keV (fix)

$T_{low} = 0.01$ keV (fix)

$M = \sim 10\ M_{sun}/yr$

[Böhringer et al. 2001, 2002; Matsushita 2002 a]

X-ray Holes Associated with Radio Lobes in the Center of the Hydra-A and Perseus Clusters

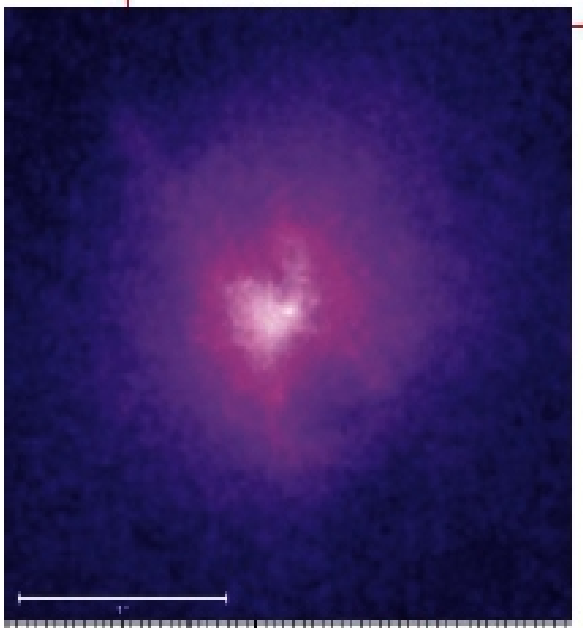

Hydra A Cluster

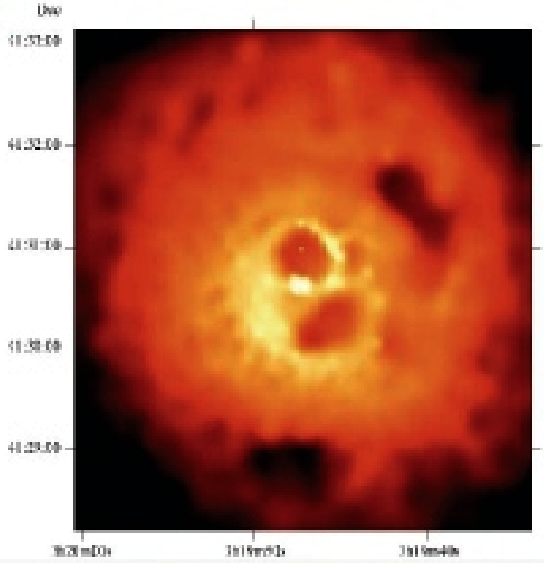

NGC 1275 in the Perseus Cluster

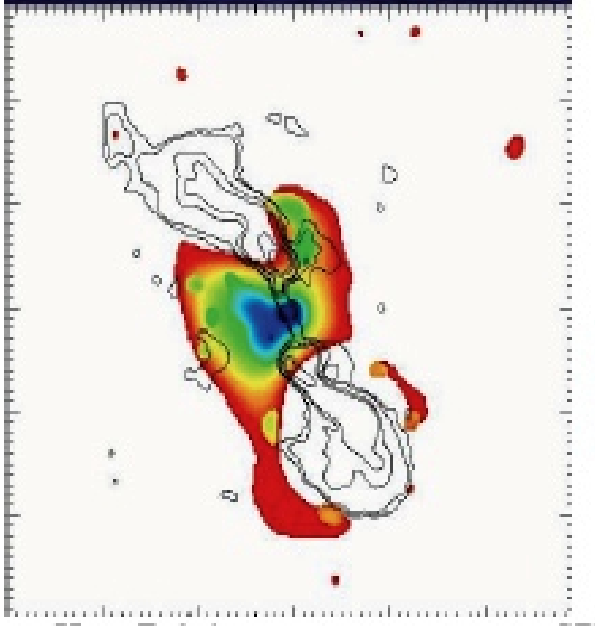

Fabian et al. 2001

McNamara et al. 2000, ApJ

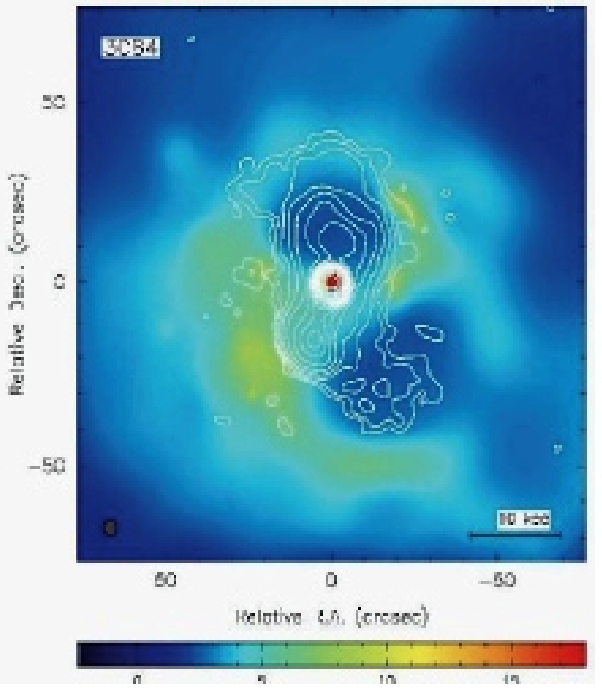

The state of the gas around low mass galaxies remains observationally largely unanswered

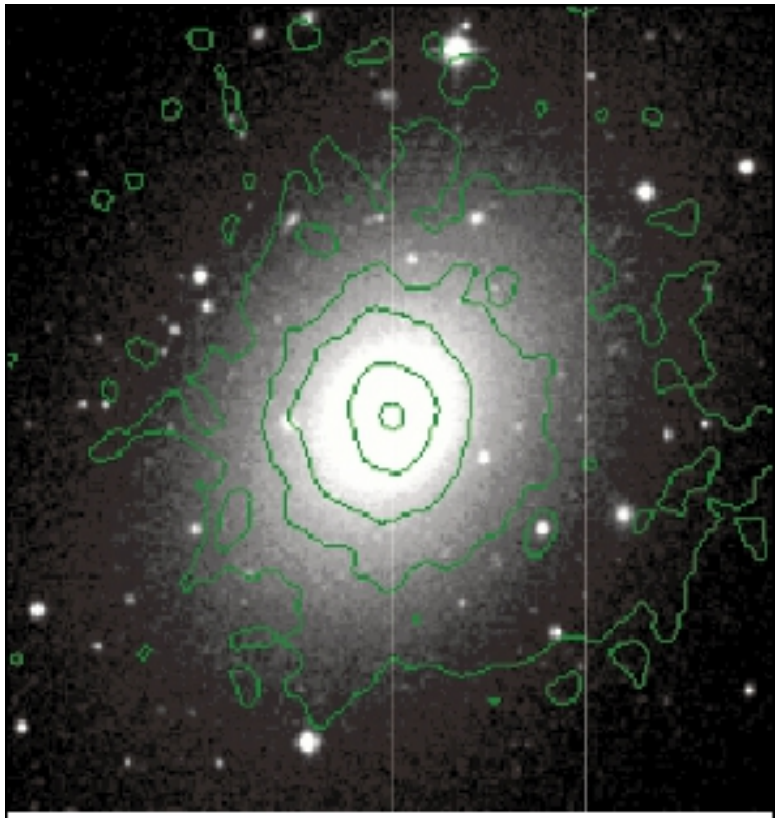

Combined X-ray and visible light emissions from NGC4636, one of nine elliptical galaxies studied by U-M astronomers. In the image shown on the Web (www.astro.lsa.umich.edu/users/jbregman), optical emissions are shown in white and X-ray emission contours are in green. Variations from the normal spectrum of starlight indicate the presence of silicates and dust grains interacting with hot gases inside the galaxy.